Expression of Interest
in

A High Luminosity Upgrade of the KEKB Collider and the Belle Detector

January 2002

I. Abe[8], K. Abe[8], T. Abe[35], I. Adachi[8], H. Aihara[36], K. Akai[8], A. Akiyama[8], K. Aoki[8], M. Arinaga[8], T. Aushev[12], S. Banerjee[33], A. Bay[16], A. M. Bakich[34], Y. Ban[28], P. K. Behera[39], I. Bizjak[13], A. Bondar[1], M. Bračko[18,13], T. E. Browder[7], P. Chang[22], B. G. Cheon[32], Y. Choi[32], Y. Doi[8], A. Drutskoy[12], K. Ebihara[8], E. Egawa[8], S. Eidelman[1], V. Eiges[12], K. Endo[8], A. Enomoto[8], E. Ezura[8], J. W. Flanagan[8], H. Fujii[8], S. Fukuda[8], H. Fukuma[8], Y. Funakoshi[8], K. Furukawa[8], T. Furuya[8], T. Gershon[8], B. Golob[17,15], A. Gordon[19], H. Guler[7], J. Haba[8], K. Hagiwara[8], K. Hara[26], T. Hara[8], T. Haruyama[8], S. Hashimoto[8], H. Hayashii[21], M. Hazumi[8], T. Higuchi[36], L. Hinz[16] S. Hiramatsu[8], H. Hisamatsu[8], T. Honda[8], H. Honma[8], K. Hosoyama[8], T. Ieiri[8], Y. Igarashi[8], N. Iida[8], T. Iijima[8], H. Ikeda[8], M. Ikeda[8], S. Isagawa[8], H. Ishii[8], H. Ishino[37], R. Itoh[8], Y. Iwasaki[8], D. J. Jackson[26], H. K. Jang[31], A. Kabe[8], T. Kageyama[8], K. Kakihara[8], S. Kamada[8], N. Kamikubota[8], T. Kamitani[8], K. Kanazawa[8], J. H. Kang[42], H. Katagiri[8], N. Katayama[8], S. Kato[8], T. Katoh[8], S. Kawabata[8], H. Kawai[3], T. Kawamoto[8], T. Kawasaki[24], H. Kichimi[8], M. Kikuchi[8], E. Kikutani[8], H. J. Kim[42], T. H. Kim[42], K. Kinoshita[5], S. Kobayashi[37], H. Koiso[8], Y. Kojima[8], I. Komada[8], P. Koppenburg[16], S. Korpar[18,15], P. Križan[17,15], T. Kubo[8], K. Kudo[8], S. Kumar[27], T. Kurimoto[38], S. I. Kurokawa[8], A. Kuzmin[1], Y.-J. Kwon[42], J. S. Lange[6], J. S. Lee[8], J. MacNaughton[11], G. Majumder[33], Y. Makida[8], A. Manabe[8], F. Mandl[11], M. Masuzawa[8], T. Matsumoto[8], S. Michizono[8], T. Mimashi[8], T. Mitsuhashi[8], S. Mitsunobu[8], K. Miyabayashi[21], H. Mizuno[8], G. R. Moloney[19], K. Mori[8], Y. Morita[8], T. Morozumi[9], T. Naito[8], T. Nakadaira[36], H. Nakai[8], H. Nakajima[8], T. T. Nakamura[8], H. Nakanishi[8], E. Nakano[25], K. Nakao[8], M. Nakao[8], H. Nakayama[8], H. Nakazawa[4], J. W. Nam[32], S. Nishida[13], S. Noguchi[21], T. Nozaki[8], J. Odagiri[8], Y. Okada[8], Y. Ogawa[8], K. Ohmi[8], T. Ohshima[20], Y. Ohnishi[8], S. Ohsawa[8], Y. Ohsawa[8], N. Ohuchi[8], K. Oide[8], S. Okuno[14], S. L. Olsen[7], M. Ono[8], T. Oogoe[8], H. Ozaki[8], T. Ozaki[8], H. Palka[23], L. S. Peak[34], J.-P. Perroud[16], M. Peters[7], L. E. Piilonen[40], S. Recksiegel[8] M. Rozanska[23], H. Sagawa[8], H. Sakai[8], Y. Sakai[8], Y. Sakamoto[8], A. Satpathy[8,5], K. Satoh[8], M. Sato[8], S. Schrenk[5], K. Senyo[20], T. Shidara[8], M. Shimamoto[8], M. Shirai[8], A. Shirakawa[8], B. Shwartz[1], J. B. Singh[27], N. Soni[27], M. Starič[13], M. Suetake[8], Y. Suetsugu[8], R. Sugahara[8], K. Sumisawa[8], T. Sumiyoshi[8], T. Suwada[8], K. Suzuki[3], S. Suzuki[41], S. Y. Suzuki[8], T. Tajima[8], F. Takasaki[8], S. Takeda[8], Y. Takeuchi[8], K. Tamai[8], J. Tanaka[36], M. Tanaka[8], M. Tanaka[26], M. Tawada[8], G. N. Taylor[19], M. Tejima[8], Y. Teramoto[25], M. Tobiyama[8], T. Tomura[36], K. Trabelsi[7], T. Tsuboyama[8], K. Tsuchiya[8], T. Tsukamoto[8], S. Uehara[8], S. Uno[8], Y. Ushiroda[8], K. E. Varvell[34], J. G. Wang[40], Y. Watanabe[37], E. Won[31], B. D. Yabsley[8], Y. Yamada[8], H. Yamamoto[35], M. Yamauchi[8], Y. Yano[8], M. Yokoyama[36], M. Yoshida[8], S. Yoshimoto[8], M. Yoshioka[8], C. C. Zhang[10], Z. Zhang[30], and F. Zimmermann[2]

[1]Budker Institute of Nuclear Physics, Novosibirsk
[2]CERN, SL Division, CH-1211 Geneva 23
[3]Chiba University, Chiba
[4]Chuo University, Tokyo
[5]University of Cincinnati, Cincinnati OH
[6]University of Frankfurt, Frankfurt
[7]University of Hawaii, Honolulu HI
[8]High Energy Accelerator Research Organization (KEK), Tsukuba
[9]Hiroshima University, Hiroshima
[10]Institute of High Energy Physics, Chinese Academy of Sciences, Beijing

[11]Institute of High Energy Physics, Vienna
[12]Institute for Theoretical and Experimental Physics, Moscow
[13]J. Stefan Institute, Ljubljana
[14]Kanagawa University, Yokohama
[15]Kyoto University, Kyoto
[16]IPHE, University of Lausanne, Lausanne
[17]University of Ljubljana, Ljubljana
[18]University of Maribor, Maribor
[19]University of Melbourne, Victoria
[20]Nagoya University, Nagoya
[21]Nara Women's University, Nara
[22]National Taiwan University, Taipei
[23]H. Niewodniczanski Institute of Nuclear Physics, Krakow
[24]Niigata University, Niigata
[25]Osaka City University, Osaka
[26]Osaka University, Osaka
[27]Panjab University, Chandigarh
[28]Peking University, Beijing
[29]Saga University, Saga
[30]University of Science and Technology of China, Hefei
[31]Seoul National University, Seoul
[32]Sungkyunkwan University, Suwon
[33]Tata Institute, Mumbai
[34]University of Sydney, Sydney NSW
[35]Tohoku University, Sendai
[36]University of Tokyo, Tokyo
[37]Tokyo Institute of Technology, Tokyo
[38]Toyama University, Toyama
[39]Utkal University, Bhubaneswer
[40]Virginia Polytechnic Institute and State University, Blacksburg VA
[41]Yokkaichi University, Yokkaichi
[42]Yonsei University, Seoul

Executive Summary

The KEKB asymmetric B-factory has achieved remarkable luminosity, 5×10^{33} cm^{-2}s^{-1}. This allowed the Belle experiment to observe CP violation in the neutral B meson system. The Belle experiment with the present KEKB will be continued until an integrated luminosity of approximately 300 fb^{-1} is accumulated. This will suffice to measure various quantities in B meson decays and study the validity of the Kobayashi-Maskawa scheme of CP violation.

As the next stage of the B-factory experiment, we consider a luminosity upgrade of the KEKB collider to extend the physics coverage. The physics opportunities at a B-factory operating at a luminosity of 10^{35} cm^{-2}s^{-1} (Super KEKB) are very attractive. The precise determination of the CKM matrix elements as well as a search for New Physics can be explored in the studies of the B meson system and the τ lepton. Super KEKB will complement the direct search for new physics at high energy colliders. Studies of rare B meson decay modes that involve neutral particles can only be performed at the e^+e^- machines.

The unprecedented luminosity of 10^{35} cm^{-2}s^{-1} appears to be feasible with a major upgrade of the existing KEKB facility. The machine can be upgraded on a time scale that makes its physics capability competitive with hadron collider experiments. The design calls for substantial amounts of research and development and pushes the accelerator technology to its limit; thus it is challenging and is a necessary step toward a new high energy e^+e^- machine.

The existing Belle detector can be upgraded in order to take full advantage of the high luminosity of the KEKB machine. Improvements in the vertex resolution, tracking and photon finding efficiencies are essential to reduce backgrounds in finding the very rare decays with missing neutral particles.

When considering the next project in the field of high energy particle physics in Japan using an accelerator, an upgrade of KEKB and Belle for the precise test of the KM mechanism and search for New Physics beyond the Standard Model in the B meson system is one of the most attractive choices. The physics motivation is very compelling and the upgrade can be achieved at a moderate cost and in a reasonable time scale.

As a consequence of these considerations, we express our interest in upgrading the KEKB collider to Super KEKB in the year 2006, accompanied by an upgrade of the Belle detector.

Contents

Chapter 1

Introduction

The KEKB asymmetric B factory project, commissioned in 1999, has achieved remarkable performance with an instantaneous luminosity of $5{\times}10^{33}$ cm^{-2}s^{-1}. An integrated luminosity of more than 40 fb^{-1}, accumulated during a two year period, allowed us to observe CP violation in the neutral B meson system. With this discovery, *i.e.* the first measurement of the CP-violating quark mixing phase, ϕ_1, the physics focus at B-factories is expected to shift to measurements of other angles of the unitarity triangle, ϕ_2 and ϕ_3, a verification of the unitarity of the CKM matrix, and to a search for effects due to new physics, particularly, but not exclusively, those induced by Supersymmetry (SUSY).

In order to accomplish these physics goals, both the accelerator and the detector performance should be upgraded. As for the accelerator, a luminosity of the order of 10^{35} cm^{-2}s^{-1} or more, which is approximately twenty times as large as the luminosity achieved at present, is required. To achieve this luminosity, the beam currents have to be increased by several factors. Since this results in shorter beam lifetimes, a substantial upgrade in injection capability becomes necessary. Also, a higher current implies more desorption, which would result in a higher vacuum pressure, which together with the more intense beams could produce dangerously high beam-induced backgrounds. The photoelectron problem, which is one of the present limitations for the beam current in the low energy ring (LER), will have to be solved by that time. On practically every front − beam current, vacuum, beam background, and injection − the luminosity requirement pushes the technology to its limit, and possibly beyond.

Apart from being able to take data at a higher rate in each subsystem, the detector should have two major improvements, better vertex resolution and a better full-reconstruction efficiency for B decays. Better vertex resolution is critical for removing continuum backgrounds that are the dominant background for interesting decay modes and in reducing combinatorial backgrounds. A better reconstruction efficiency comes from improved hermiticity of the detector and plays a central role in the technique of full-reconstruction tagging, which may be the only method to observe some of the rare decays that involve neutral particles. In the environment of B-factories, to improve vertex resolution requires a smaller beampipe radius, which means a battle with beam backgrounds. Such an effort requires close coordination between the accelerator and detector groups.

When the 10^{35} cm^{-2}s^{-1} machine comes into existence, we must compete with experiments at hadron colliders, such as $LHCb$ and $BTeV$. Those hadronic machines can produce large quantities of B mesons and in some channels, such as $B \to \mu^+\mu^-$ it is difficult for an e^+e^- machine to compete. However, for many of the critical channels,

such as $B \to K\nu\bar{\nu}$, $B \to D\tau\bar{\nu}$, and $B \to \pi^0\pi^0$ - namely, modes with missing neutrinos or with gammas - an e^+e^- machine has definite advantages. In fact, some of those modes are expected to be observable only at an e^+e^- machine. An e^+e^- B-factory at 10^{35} cm^{-2}s^{-1}, Super KEKB, is a natural extension of the KEKB/Belle project that has achieved remarkable success in the field of High Energy Physics.

In this report, we express our interest in upgrading the KEKB collider to a machine with L =10^{35} cm^{-2}s^{-1} (Super KEKB), as described in Chapter 3, in the year 2006 to carry out the physics program described in detail in Chapter 2. The Belle detector needs to be upgraded at the same time, which is described in Chapter 4.

Chapter 2

Physics Motivations

Historically, flavor mixing and CP violation have played important roles in our understanding of the laws of elementary particles. SU(3) flavor symmetry and Cabibbo mixing are fundamental concepts of the strong and weak interactions of light hadrons. In fact, the suppression of flavor changing neutral current processes in the kaon system led us to the existence of the charm quark. Furthermore, even before the discovery of the charm quark, Kobayashi and Maskawa proposed a third generation of quarks and a flavor mixing matrix in order to explain the CP violation observed in $K^0 - \bar{K}^0$ mixing [1]. The KM model of CP violation has become one of the essential building blocks of the Standard Model. Since the complex phase of the Cabibbo-Kobayashi-Maskawa (CKM) matrix is the only source of the CP violation in the quark flavor transition within the Standard Model, a measurement of the CP violation outside the kaon system provides a crucial test of the Kobayashi-Maskawa mechanism.

Recently, Belle at KEKB and BaBar at PEP-II have observed CP violation for the first time outside the kaon system. They use asymmetric colliders to measure the time-dependent CP asymmetry in B decays [2, 3, 4]. A large CP asymmetry recently observed in the $B \to J/\psi K_S$ and other $(c\overline{c})K_{S,L}$ modes [5, 6] is consistent with the constraints from the Kobayashi-Maskawa mechanism. The success of these experiments leads to a new method for exploring physics beyond the Standard Model. Since various observable quantities in K and B meson decays are governed by the same CKM matrix elements in the Standard Model, quantitative tests of the Standard Model can be performed by making measurements of CP asymmetries in B decays and of rare B decay processes. If we observe some deviation from the Standard Model, we will be able to obtain important clues to discover the underlying new physics.

Within a few years, the precision of $\sin 2\phi_1$ in the unitarity triangle will be greatly improved by the Belle experiment, and the CP asymmetries in other modes, such as $B \to K\pi$ and $B \to \pi\pi$, will also be observed. Among the rare decay processes, the branching ratio of an exclusive $b \to s\ell^+\ell^-$ mode, $B \to K\mu^+\mu^-$ has been already observed [7]. It will then become clear whether or not the main source of the flavor mixing and CP violation in the quark sector comes from the KM mechanism.

The goal of the experiment at Super KEKB is a precise determination of the CKM matrix elements as well as searches for new physics through measurements of CP violation and rare decay processes in B meson decays. Although one of the angles of the unitarity triangle, $\sin 2\phi_1$, will be determined up to an accuracy of a few %, and the other angles, ϕ_2 and ϕ_3, will also be studied in the current B factory experiments, we need at least

a factor of ten times more luminosity for precise measurements of these angles. As for the rare decays, a precise measurement of the lepton forward-backward asymmetry of the $b \to s\ell^+\ell^-$ processes, for example, is possible only with such a high luminosity. These precise measurements are not only important to over-constrain the unitarity triangle, but are also essential to search for new physics effects and to distinguish various models beyond the Standard Model. It may be possible that hints for new physics will be obtained in the current B factories. However, to disentangle observed deviations from the Standard Model and to clarify their physical meanings, we definitely need a second stage B-factory experiment.

Examples of important measurements at Super KEKB are listed below:

- Further precise measurement of $\sin 2\phi_1$,
- Time-dependent CP asymmetry of $B \to \phi K_S$ to search for phases from new physics,
- $B \to \pi\pi$ and $B \to \rho\pi$ including $\mathcal{B}(B^0 \to \pi^0\pi^0)$ for the isospin analysis to measure $\sin 2\phi_2$,
- $B^\pm \to DK^\pm$ for ϕ_3,
- $B^0(\overline{B}^0) \to D^{(*)+}\pi^-$ for $\sin(2\phi_1 + \phi_3)$,
- $B^0(\overline{B}^0) \to D^{*+}\rho^-$ with angular analysis for $\sin(2\phi_1 + \phi_3)$,
- $|V_{ub}|$ measurements from inclusive and exclusive $b \to u\ell\nu$ decays,
- Inclusive and exclusive $b \to s\ell^+\ell^-$ decays,
- Inclusive and exclusive $b \to s\nu\bar{\nu}$ decays,
- Direct CP violation of $b \to s\gamma$ and $b \to d\gamma$,
- Time-dependent CP asymmetry of $B \to K_1\gamma$ and $B \to \rho\gamma$,
- Branching fractions and τ polarizations in $B \to D^{(*)}\tau\nu$,
- $B \to \tau\nu$ and $B \to \mu\nu$, and
- $B \to \tau^+\tau^-$ and $B \to \mu^+\mu^-$.

In addition to these B decay processes, the B-factory will produce more than 10^9 τ and charmed particles per year. These may be used to search for new physics through lepton flavor violating decays of tau particles, such as $\tau \to \mu\gamma$ and $\tau \to 3\mu$, or through $D^0 - \bar{D}^0$ mixing.

2.1 Unitarity Triangle

In the Standard Model, the flavor mixing in the quark sector is described by a mixing matrix in the charged current interaction,

$$\mathcal{L} = -\frac{1}{\sqrt{2}}\bar{u}_{iL}\gamma^\mu V_{ij} d_{jL} W_\mu + h.c., \tag{2.1}$$

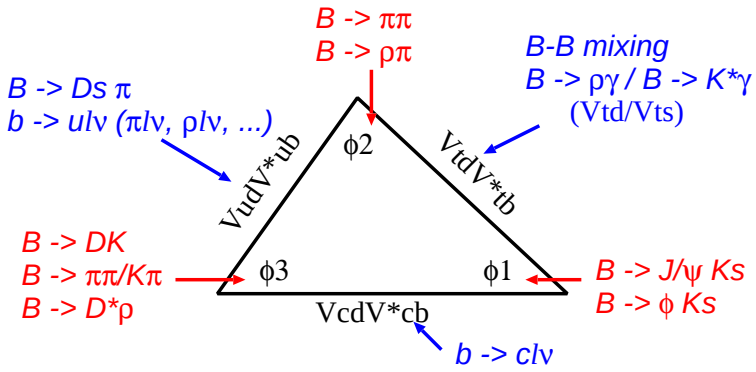

Figure 2.1: Unitarity triangle with various observables in B decays.

where V_{ij} is a CKM matrix element. The CKM matrix is unitary, and one of the unitarity constraints is expressed as

$$V_{td}V_{tb}^* + V_{cd}V_{cb}^* + V_{ud}V_{ub}^* = 0. \tag{2.2}$$

Normalizing by $V_{cd}V_{cb}^*$, this constraint is represented as a triangle in the complex plane, which is called the unitarity triangle. The upper vertex corresponds to the coordinate (ρ, η), where ρ and η are two of four independent parameters of the CKM matrix in the Wolfenstein parameterization:

$$V = \begin{pmatrix} 1 - \frac{1}{2}\lambda^2 & \lambda & A\lambda^3(\rho - i\eta) \\ -\lambda & 1 - \frac{1}{2}\lambda^2 & A\lambda^2 \\ A\lambda^3(1 - \rho - i\eta) & -A\lambda^2 & 1 \end{pmatrix} + \mathcal{O}(\lambda^4). \tag{2.3}$$

The lengths and angles of the unitarity triangle can be determined from various measurements in B decays, as shown in Fig. 2.1.

The present experimental status of the unitarity triangle determination is summarized in Fig. 2.2. The two parameters, ρ and η, are constrained by five quantities: the CP violation parameter in the $K^0 - \bar{K}^0$ mixing (ϵ_K), the $B_d^0 - \bar{B}_d^0$ mass difference ($\Delta M_{B_d^0}$), $|V_{ub}|$ through $b \to u\ell\bar{\nu}$ decay rate, the lower bound of $B_s^0 - \bar{B}_s^0$ mixing ($\Delta M_{B_s^0}$), and $\sin 2\phi_1$ from the time dependent CP asymmetry in B decays.

By 2006 we expect that the measurement error of $\sin 2\phi_1$ will be reduced to the 5% level, and that $\Delta M_{B_s^0}$ will be measured by Tevatron Run II experiments. The four-fold ambihuity in ϕ_1 calculated from $\sin 2\phi_1$ can be solved by measureing $\cos 2\phi_1$ in the decay modes such as $B^0 \to D^{(*)+}D^{(*)-}K_S$. Therefore, the two parameters, ρ and η, will be precisely known before the Super KEKB experiment starts as long as we assume the Standard Model. Deviations from the constraints in the (ρ, η) plane, deduced from other measurements, offer a promising way to look for new physics.

In the experiment at Super KEKB, we aim to improve the constraints given above and to add more constraints from new measurements. In doing so, it is essential to reduce the theoretical uncertainties in the measurements of the angles and lengths of the unitarity triangle; otherwise, the the Standard Model cannot be thoroughly tested. Many ideas on how to perform theoretically clean determinations have been proposed in the literature. Among them, we consider the theoretical and experimental feasibilities of the following measurements in the Super KEKB experiment.

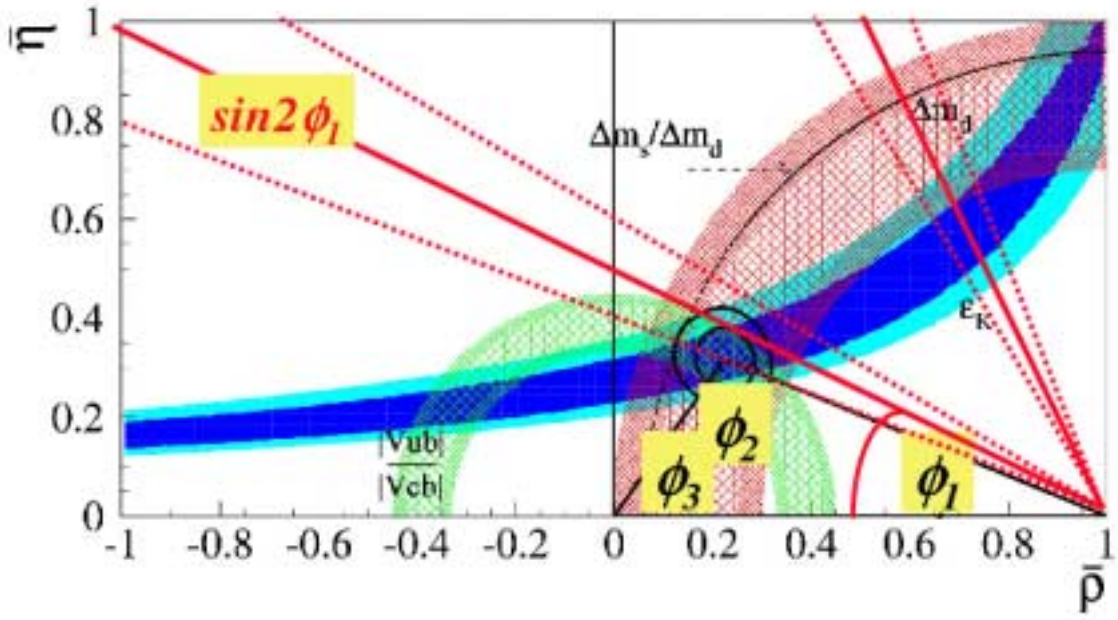

Figure 2.2: Present status of the constraint on the unitarity triangle [9].

2.1.1 $\sin 2\phi_1$ measurement and search for phases from new physics

A precise measurement of $\sin 2\phi_1$ is essential to determine the complex phases of the CKM matrix elements. Furthermore, it may even be possible to obtain some evidence of new physics by making several measurements of $\sin 2\phi_1$ in different modes.

The measurement of $\sin 2\phi_1$ through $B \to J/\psi K_S$, $B \to J/\psi K_L$ and $B \to J/\psi K^*$ has the unique feature that there is little theoretical uncertainty within the framework of the Standard Model, because the tree and penguin decay diagrams in the $b \to c\bar{c}s$ transition both have the same weak phases to a very good approximation. In the Standard Model, the possible correction is at the 1% level, or less. If this assumption is violated by some new physics contribution, a sizable direct CP asymmetry may be induced. It is therefore interesting to determine both the $\sin(\Delta mt)$ and $\cos(\Delta mt)$ terms in the time-dependent asymmetry in these modes with at the few % level of uncertainty.

We can also look for a new CP violating phase by measuring the time-dependent asymmetries in the neutral B meson decays governed by different quark level diagrams from that for $J/\psi K_S$, such as;

- $B^0 \to \phi K_S$ and $\eta' K_S$ ($b \to s\bar{s}s$),
- $B^0 \to D^{(*)+} D^{(*)-}$ and $J/\psi\pi^0$ ($b \to c\bar{c}d$), and
- $B^0 \to D^0(\to f_{CP})h^0$, where f_{CP} denotes a CP eigenstate such as K^+K^- and h^0 is π^0, η, η' or ω ($b \to c\bar{u}d$).

In the Standard Model, the CP asymmetry from the dominant decay diagram is the same for these modes, while the sub-dominant part may develop different weak phases. An especially interesting example is $B \to \phi K_S$, which occurs through a b to s penguin diagram; the CP asymmetry is the same as that of the $B \to J/\psi K_S$ to a very good approximation within the Standard Model. However, if there are new physics contributions in the penguin diagram with different CP phases, the asymmetry can be different. Such new CP violation phases may arise in SUSY models, for instance [10, 11, 12]. At the moment, such new phases are unconstrained.

2.1.2 $\sin 2\phi_2$ from $B \to \pi\pi$ and $B \to \rho\pi$

The angle ϕ_2 is determined by the time-dependent CP asymmetry of a tree $b \to u\bar{u}d$ transition, such as $B^0(\overline{B}^0) \to \pi^+\pi^-$. In this case, however, a problem known as the penguin pollution exists. Namely, there are sizable contributions from penguin diagrams, which develop different weak phases from the tree transition, and therefore the CP asymmetry measured in the experiment may not be directly related to $\sin 2\phi_2$. In order to extract $\sin 2\phi_2$ in a theoretically clean way by separating the contribution of the tree amplitude from that of the penguin amplitude, one must rely on isospin relations, which require measurements of all $B \to \pi^{\pm,0}\pi^{\pm,0}$ modes [13]. In particular the measurement of the branching ratio for $B^0 \to \pi^0\pi^0$ is challenging because it is small, *i.e.* it is expected to be at the 10^{-6} level, or below. It can only be measured at a higher luminosity e^+e^- B-factories. This will be the theoretically cleanest way of determining $\sin 2\phi_2$.

The parameter $\sin 2\phi_2$ can also be obtained from $B \to \rho\pi$ modes with isospin relations [14]. The time-dependent Dalitz distribution of three pion final states allows us to disentangle the tree amplitude. This measurement also requires high luminosity.

2.1.3 ϕ_3 from $B \to DK$

The angle ϕ_3 will be determined using the $B \to DK$ mode. The amplitudes of $B^+ \to \bar{D}^0 K^+$ and $B^+ \to D^0 K^+$ are proportional to $V_{cb}^* V_{us}$ and $V_{ub}^* V_{cs}$, respectively. If we choose a final state which can be reached both from $\bar{D}^0 K^+$ and $D^0 K^+$, ϕ_3 can be determined from their interference. Although the original method of Gronau and London [15] and Gronau and Wyler [16], where only CP eigenstates of D meson are used, has experimental difficulty, the modified method proposed by Atwood, Dunietz and Soni [17, 18] would provide us with a theoretically clean way to determine ϕ_3. Since the solution for ϕ_3 has a discrete ambiguity, it more than 1,000 fb^{-1} is needed to obtain practically useful information on ϕ_3.

2.1.4 $\sin(2\phi_1 + \phi_3)$ from $B \to D^{(*)}\pi$ and $B \to D^*\rho$

Another promising way to determine ϕ_3 is a measurement of the time-dependent asymmetries in $B \to D^{(*)}\pi$ mode [19]. The decay processes $B^0 \to D^{*+}\pi^-$ and $\bar{B}^0 \to D^{*+}\pi^-$ occur through $\bar{b} \to \bar{u}c\bar{d}$ and $b \to c\bar{u}d$ quark diagrams and their amplitudes are proportional to $V_{ub}^* V_{cd}$ and $V_{ud}^* V_{cb}$, respectively. The measurement of the time-dependent asymmetries in the $B^0 \to D^{*+}\pi^-$ and $B^0 \to D^{*-}\pi^+$ modes may be used to extract $\sin(2\phi_1 + \phi_3)$ and the strong phase difference of the two amplitudes in a theoretically clean way, although there is a discrete ambiguity to solve for these angles. In this method, however, we need to measure the square of the smaller amplitude, although the magnitudes of two amplitudes are expected to be quite different [20].

Recently, London, Sinha and Sinha proposed a time-dependent angular analysis of the $B \to D^*\rho$ mode [21]. In the vector-vector decay of a B meson, there are three independent amplitudes according to the spin-spin correlation of the two vector mesons. These three amplitudes as well as interference terms can be determined using a full angular analysis of the decay products of the two vector mesons. It is shown that a method similar to that used for $B \to D^{(*)}\pi$ can be applied to this case in order to extract $\sin(2\phi_1 + \phi_3)$. Moreover, this mode has the advantage that we do not have to measure the square of the smaller amplitudes because information on interference terms is sufficient to determine $\sin(2\phi_1 + \phi_3)$.

2.1.5 Direct CP asymmetry of $B \to K\pi, \pi\pi$

The branching ratios of the $B \to K\pi$ modes are relatively large because of large contributions from the b to s penguin diagram. Although there can be sizable direct CP asymmetries, there may be a large theoretical uncertainty in the extraction of information on the weak phase. There have been several proposals, e.g. Neubert and Rosner [22], to constrain ϕ_3 by invoking SU(3) relations.

Another approach is to calculate the decay amplitudes of exclusive processes by the perturbative QCD method [23, 24, 25]. In this approach, the strong phase is estimated from the imaginary part of quark diagrams, so that both branching ratios and direct CP asymmetries are calculable. In the B-factory experiment, it will be known how well these approaches can reproduce the experimental observables. Direct CP asymmetries in $B \to K\pi, \pi\pi$ may become important for determining the angles in the unitarity triangle as well as for searching for new physics contributions.

2.1.6 $|V_{ub}|$ measurement

In order to over-constrain the unitarity triangle, the precise determination of the lengths of the sides is as important as angle measurements. The present determinations of $|V_{ub}|$ use the total decay rate of an inclusive process $b \to u\ell\nu$. This measurement contains large uncertainty due to the assumption made in the differential decay rate as one has to apply a cut to avoid a background from $b \to c\ell\nu$. In the Super KEKB experiment, however, the higher luminosity and better energy resolution allow us to use less restrictive cuts on the momentum and invariant mass distributions of decay products to minimize the theoretical uncertainty.

Exclusive semi-leptonic processes, such as $B \to \pi\ell\nu$ and $B \to \rho\ell\nu$, may be used to determine $|V_{ub}|$, provided that the form factors are reliably calculated with non-perturbative methods. Lattice QCD is the most promising method, which does not depend on any hadronic model. Although the currently available lattice calculations of the relevant form factors [26, 27, 28, 29] contain large systematic uncertainties due to limited computing power, we expect considerable improvements in the next several years. Since the lattice QCD is reliable only in the large-q^2 region, which corresponds to a small recoil of the daughter hadrons, a precise experimental measurement of the differential decay rate is required to determine $|V_{ub}|$.

Another method is to measure the decay rate $B \to X_u\ell\nu$ inclusively. If tight cuts on kinematical variables are applied to avoid background from the much larger $B \to X_c\ell\nu$ transition, the theoretical uncertainty becomes large, because it relies on an extrapolation using a theoretical model. Several strategies have been proposed in order to minimize the model dependence in the theoretical calculation of the decay rate, and a determination of $|V_{ub}|$ of order 10% is possible [30, 31, 32, 33]. Since these methods use cuts on the hadron invariant mass or lepton invariant mass distributions, reconstruction of a neutrino four-momentum is required. Given the low efficiency of neutrino reconstruction, a high luminosity e^+e^- B-factory is the only possibility for the precise determination of $|V_{ub}|$.

2.2 Rare B Decays

2.2.1 $b \to s\ell^+\ell^-$ and $b \to s\nu\bar{\nu}$

The rare decay processes $b \to s\ell^+\ell^-$ and $b \to s\nu\bar{\nu}$ are ideal places to look for new physics. In the Standard Model, these Flavor Changing Neutral Current (FCNC) processes are induced by one-loop diagrams involving an internal top, charm or up quark. New physics may affect these processes through additional contributions to the loop diagrams and/or tree-level FCNC Z boson couplings.

The current status of exclusive branching fraction measurements of $b \to s\ell^+\ell^-$ transitions is shown in Fig. 2.3 together with the Standard Model predictions. The Belle experiment has recently measured the branching ratio for the $K\mu^+\mu^-$ mode [7]. The measurement of the inclusive $b \to s\ell^+\ell^-$ branching ratio is also important, because the inclusive mode has much smaller theoretical uncertainties.

In order to discriminate different models of new physics, the dilepton invariant mass distribution and the lepton forward-backward (FB) asymmetry are useful for both inclusive and exclusive measurements. For example, effects of SUSY particles have been investigated [34, 35, 36, 37, 38]. In Figs. 2.4 and 2.5, the spectrum and the FB asymmetry

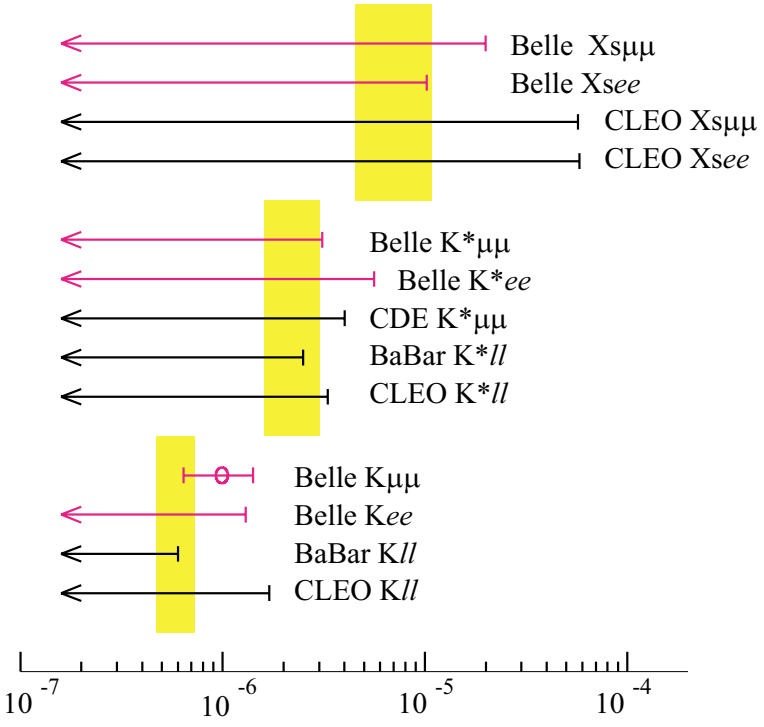

Figure 2.3: Recent status of $b \to s\ell^+\ell^-$ processes. The shaded bands are predictions of the Standard Model.

of the inclusive $b \to s\ell^+\ell^-$ are shown for the Standard Model and a particular parameter point of the minimal supergravity model where the $b \to s\gamma$ amplitude has an opposite sign to the Standard Model prediction. A clear difference is seen between the two cases. In particular, the lepton FB asymmetry changes its sign between low and high dilepton invariant mass in the Standard Model, while its sign is the same for the other case. It was shown that a similar asymmetry is useful to distinguish two cases for the exclusive $B \to K^*\ell^+\ell^-$ mode. In the Standard Model the lepton invariant mass where the asymmetry changes its sign is relatively stable for different choices of the form factors [39]. We can also use the azimuthal angle distribution in $B \to K^*(\to K\pi)\ell^+\ell^-$ to probe new physics effects [40].

The branching ratio of $b \to s\tau^+\tau^-$ is expected to be one order of magnitude smaller than those of $b \to se^+e^-$ or $b \to s\mu^+\mu^-$, and its measurement is experimentally more challenging because at least two neutrinos are involved. From a theoretical point of view, this process is interesting because one can measure the tau polarization. The measurement of tau polarization will provide us with additional information to disentangle new physics effects [41].

The $b \to s\nu\bar{\nu}$ process is also induced by one-loop diagrams in the Standard Model. Unlike $b \to s\ell^+\ell^-$, there is no interference effect between the J/ψ and ψ' resonances. The inclusive branching ratio is expected to be 4.1×10^{-5} in the Standard Model. Since the theoretical uncertainty is small, experimental measurements are very important to search for new physics. This measurement will be possible only at e^+e^- B factories with good efficiency for full reconstruction. Exclusive processes, such as $B \to K\nu\bar{\nu}$ and $B \to K^*\nu\bar{\nu}$,

Figure 2.5: Lepton forward-backward asymmetry for the Standard Model at the same parameter point of the minimal supergravity model as in Fig. 2.4 [37].

are also interesting. In these modes, the relevant form factors may be calculated by lattice QCD, or evaluated from the known form factors of $B \to \pi\ell\nu$ and $B \to \rho\ell\nu$ using SU(3) relations. The $\nu\bar{\nu}$ invariant mass spectrum as well as K^* polarization are useful to distinguish new physics effects from the Standard Model [42].

2.2.2 Radiative B decays

The branching ratio of the inclusive $b \to s\gamma$ decay and of some exclusive modes have already been measured experimentally. At the B-factory with a luminosity of over 10^{35} cm^{-2}s^{-1}, the properties of the $b \to s\gamma$ processes will be precisely measured. At this stage, measurements of CP violation in both inclusive and exclusive modes offer interesting opportunities for a new physics search.

The direct CP asymmetry of the inclusive $b \to s\gamma$ process is suppressed in the Standard Model, since all diagrams contributing to this process have almost the same weak phases. The asymmetry is then expected to be less than 1%. On the other hand, if there is a new CP phase in the loop diagrams, the asymmetry can be larger, and in some case it is close to 10%. One such example is given by the SUSY model where new CP violating phases in the SUSY breaking sector are introduced [43, 44, 45, 46].

The time-dependent asymmetry of exclusive modes, for example the $B^0 \to K_1\gamma$ mode, is also interesting to search for new physics. CP asymmetry can arise if both $b \to s\gamma_L$ and $b \to s\gamma_R$ decay amplitudes exist. In the Standard Model, this asymmetry is suppressed by m_s/m_b, so that it can only be a few %. On the other hand, if new physics enhances the $b \to s\gamma_R$ amplitude, the asymmetry can be $O(1)$[47, 48]. For example, the asymmetry can be 20% in a SUSY GUT model with a right-handed neutrino, since the neutrino flavor mixing can be a source of flavor mixing in the right-handed-down-type squark sector [49, 50].

The $b \to d\gamma$ transition is also important. The branching ratios for inclusive and exclusive processes are expected to be smaller by one or two orders of magnitudes than those for the $b \to s\gamma$ process. In the Standard Model, measurements of $B \to \rho\gamma$ and $B \to \omega\gamma$ processes are useful to obtain information on $|V_{td}|$. In addition, direct CP asymmetries for both inclusive and exclusive processes are much larger compared to those in $b \to s\gamma$ [51, 52, 53]. Both the branching ratio and the direct asymmetry are useful to search for new physics [54, 55, 56, 57, 58]. The time-dependent asymmetry in $B^0 \to \rho\gamma$ is expected to be small in the Standard Model, so that it is a sensitive probe for new contributions to the $b \to d\gamma$ amplitude [47].

2.2.3 Tauonic B decay

B decays to final states with a τ lepton include $B \to D^{(*)}\tau\nu$, $B \to \tau\nu$ and $B \to \tau^+\tau^-$. All of these decays involve more than one neutrino in the final state, so that good hermeticity of the detector is required for their measurement. Among them $B \to D^{(*)}\tau\nu$ and $B \to \tau\nu$ occur at the tree level, and $B \to \tau^+\tau^-$ is generated by a one-loop diagrams. The process $B \to \tau\nu$ is important for a direct measurement of the B meson decay constant (f_B) in conjunction with the $|V_{ub}|$ measurement.

The decay $B \to D^{(*)}\tau\nu$ is interesting for new physics searches. This process is sensitive to the existence of a charged Higgs boson, like in the case of the Minimal Supersymmetric Standard Model (MSSM) [59]. This is particularly important, because, unlike the non-

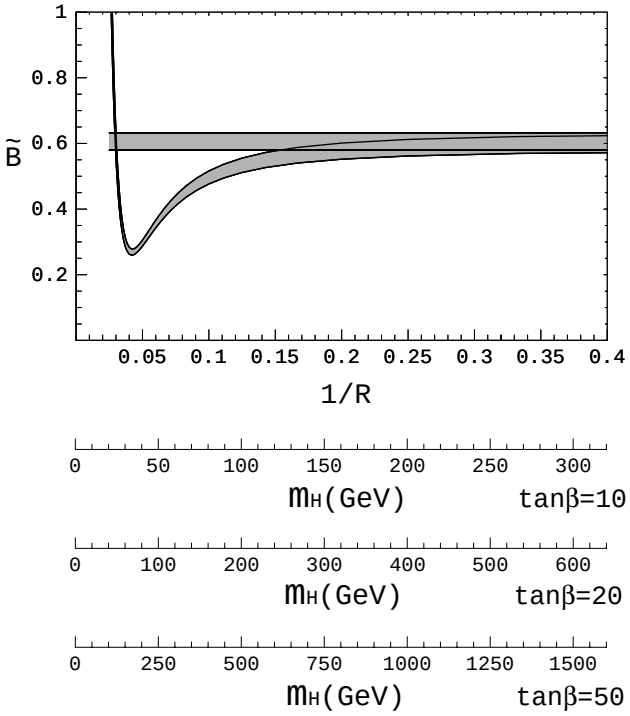

Figure 2.6: Ratio of $\Gamma(B \to D\tau\nu)$ to $\Gamma(B \to D\mu\nu)$. The flat band is the prediction of the Standard Model, while another one includes the charged Higgs contribution shown as a function of the charged Higgs mass and $\tan\beta$ [60]. The width of the band is due to uncertainty in the form factor.

SUSY type-II two Higgs doublet model, the charged Higgs mass is not strongly constrained by the branching ratio of the $b \to s\gamma$ process due to possible destructive interference between SUSY loop diagrams and the charged-Higgs-boson loop diagram. In the theoretical calculation, we can use information on relevant form factors from the $B \to D^{(*)}l\nu$ process and the heavy quark symmetry. Since the charged Higgs boson effect is enhanced for a large value of $\tan\beta$, which is the ratio of two Higgs vacuum expectation values, we can put an important constraint on the m_A–$\tan\beta$ parameter space (m_A is a CP-odd Higgs boson mass) as shown in Figs. 2.6 and 2.7 [60].

2.3 Tau Physics

At the B-factory experiment with a luminosity of over $10^{35}\mathrm{cm}^{-2}\mathrm{s}^{-1}$ more than 10^9 τ pairs per year will be produced. Among various tau physics which can be carried out, a search for lepton flavor violation is one of the important possibilities.

In the Standard Model, the lepton number is conserved separately for each generation if we neglect the neutrino masses. Furthermore, a simple model of neutrino mass generation, such as the see-saw model, does not generate charged lepton flavor violation processes at an experimentally accessible level, although the neutrino oscillation implies that lepton flavor conservation is not exactly valid. Therefore, an observation of the lepton flavor violation would be a clear signal for physics beyond the Standard Model with simple extensions to incorporate the neutrino mass generation.

Searches for lepton flavor violation have been carried out in both the τ and μ decay

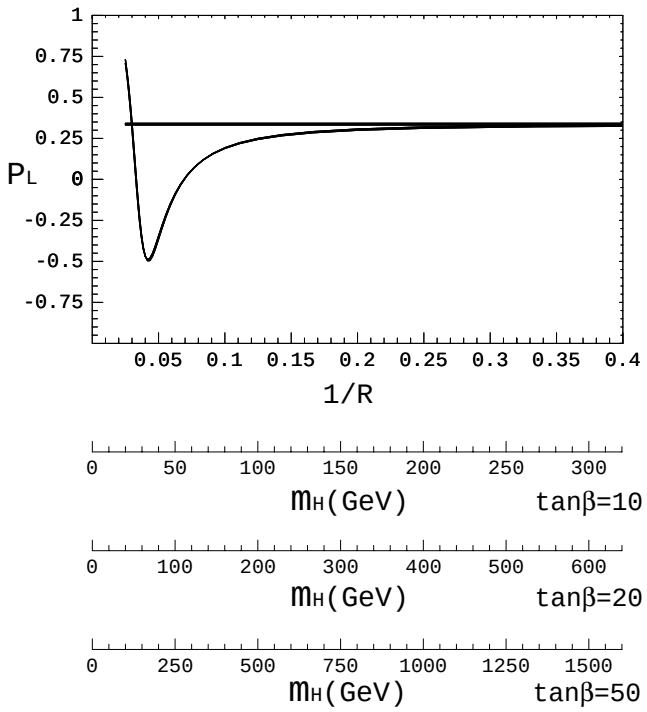

Figure 2.7: Polarization of τ in $B \to D\tau\nu$ decay. The flat band is the prediction of the Standard Model, while the curve includes the charged Higgs contribution shown as a function of the charged Higgs mass and $\tan\beta$ [60]. The theoretical uncertainty in the form factor is negligibly small.

processes. Although the upper-bound of $\mu \to e\gamma$ branching ratio is $O(10^{-11})$, and those for $\tau \to \mu\gamma$ and $\tau \to 3\mu$ are $O(10^{-6})$, theoretical predictions on these branching ratios are model-dependent. For example, it has been pointed out that in some models of SUSY GUT and SUSY with right-handed neutrino the expected branching ratios can be close to the present experimental bounds for both τ and μ processes [61, 62, 63]. Improvements of the branching ratios by one or two orders of magnitude are therefore very interesting.

In addition to the branching ratio, we can obtain information on P and T odd asymmetries in $\tau \to \mu\gamma$ and $\tau \to 3\mu$ decays, if we use spin-spin correlations of tau pairs [64]. Such a measurement offers an interesting way to distinguish different models with lepton flavor violation.

The CP properties of the third fermion family are largely unexplored. The b-quark hadronizes before it decays, and its properties are difficult to probe directly. The t-quark decays before hadronization, and hence its CP properties can be studied through its decay angular distributions. The production and decay of the τ lepton offer a particularly clean laboratory to study its CP properties. A measurement of the τ electric dipole moment (EDM) and that of the CP violating effects in τ semileptonic decays should be performed at both present and future B factories.

The weak EDM of τ, the EDM-like coupling of the τ lepton to the Z-boson has been measured accurately at LEP1, $d_\tau^W < 5.6 \times 10^{-18}\mathrm{e}\cdot\mathrm{cm}$ (95% CL) [65], whereas the constraint on the τ EDM is still mild, $d_\tau < 3.1 \times 10^{-16}\mathrm{e}\cdot\mathrm{cm}$ (95% CL) [65]. With 10^9 τ pair events, the sensitivity to the τ EDM should reach the level of $0.2 \times 10^{-18}\mathrm{e}\cdot\mathrm{cm}$ [66], a three-orders of magnitude improvement over the present EDM measurement, and a far

better than the present weak moment measurement.

Semileptonic decays of τ may offer laboratories for detecting new CP violation effects. Here, typically one measures the branching-fraction asymmetry between a τ^- semileptonic decay mode and its CP conjugate decay mode of τ^+. New physics that couples to the weak currents with the Lorentz property different from the Standard Model should provide us with a CP violating phase, and typically the interference between two or more Breit-Wigner resonance phases makes CP-odd asymmetries to be observable. Theoretical predictions based on multiple Higgs boson models and lepto-quark exchange models appear in the literature for the 3π mode [67], the $K\pi$ mode [68, 69], and for the $K\pi\pi$ and $KK\pi$ modes [70].

2.4 Charm Physics

At a B factory, a large number of charm mesons are produced from the $q\bar{q}$ continuum and also from decay products of B mesons. For example, with 11.1 fb^{-1} Belle reconstructs 10^5 D^0 ($\bar{D}^0$), 8×10^3 $D^\pm$ and 6×10^3 $D_s^\pm$ mesons in low multiplicity decay modes. We can expect data samples a hundred times larger with a luminosity of $10^{35}\,\mathrm{cm}^{-2}\mathrm{s}^{-1}$.

Due to the effectiveness of the GIM mechanism, flavor-changing neutral current (FCNC) decays, $D^0 - \bar{D}^0$ mixing and CP violation are small in the charm sector. This is in sharp contrast with K and B FCNC processes, which are enhanced by the presence of top quarks in loops. In many cases, extensions of the Standard Model (SM) upset this suppression and give contributions sometimes orders of magnitude larger than the SM. As a result, rare charm processes are an excellent place to look for new physics.

The strength of $D^0 - \bar{D}^0$ mixing is characterized by two parameters $x = \Delta M/\Gamma$ and $y = \Delta\Gamma/2\Gamma$. According to the conventional expectation of the SM, $x, y \leq 10^{-3}$. However, in a recent treatment by Falk *et al.*, the possibility of y (and perhaps x) $\sim 10^{-2}$ within the SM is raised [71]. The current experimental limits are at the level of a few times 10^{-2}.

Experimental searches for $D^0 - \bar{D}^0$ mixing usually involve hadronic decay modes such as $D^0 \to K^+\pi^-$. For such modes, there are contributions from both mixing and doubly Cabibbo suppressed decays (DCSD), which can be distinguished by their time dependences. In the CP conserving limit, the rate for wrong sign decays is

$$r_{WS}(t) = [R_D + \sqrt{R_D}y't + 1/4(x'^2 + y'^2)t^2]e^{-t},$$

where R_D is the DCSD rate, and $y' = y\cos\delta - x\sin\delta$ and $x' = x\cos\delta + y\sin\delta$ are the mixing parameters y and x rotated by δ, the relative strong phase between $D^0 \to K^+\pi^-$ and $\bar{D}^0 \to K^+\pi^-$. In the absence of interference, mixing has a t^2e^{-t} dependence which peaks at 2 D^0 lifetimes, whereas DCSD follows the usual e^{-t} dependence. The interference term is proportional to te^{-t} and dominates the sensitivity to mixing, since $(x'^2 + y'^2) = (x^2 + y^2) \ll R_D$. Since the measurement of y' and x' requires that these three terms be distinguished from each other, decay-time resolution is crucial: improved vertexing at the Belle upgrade, together with the very large D^0 samples available at $10^{35}\,\mathrm{cm}^{-2}\mathrm{s}^{-1}$, will lead to an improvement in sensitivity over previous experiments [72] and the existing B-factories.

Interpretation of $D^0 \to K^+\pi^-$ and other hadronic-decay mixing analyses is complicated by the strong phase difference δ, which may be large [73],[74]: it is important to obtain constraints on this quantity. At a tau-charm facility, δ can be determined by using

quantum correlations with two fully reconstructed D decays [75]. At a high luminosity B factory, δ can be determined by measuring related DCSD modes, including modes with K_L mesons [76].

If CP is violated in the D system, then additional $D^0 - \bar{D}^0$ mixing signals may be seen. CP violation in the interference of D^0 decays with and without $D^0 - \bar{D}^0$ mixing is parameterized by the phase $\phi_D = \arg(q/p)$: the SM expectation is $\mathcal{O}(10^{-3} - 10^{-2})$, whereas in new physics scenarios it can be $\mathcal{O}(1)$. This is in contrast with direct CP violation, which occurs in Cabibbo suppressed decays such as $D \to \rho\pi$ at the 10^{-3} level in the SM: new physics scenarios are unlikely to change this expectation.

A time dependent asymmetry

$$\Gamma(D^0(t) - \bar{D}^0(t)) \propto x \sin\phi_D \Gamma t e^{-\Gamma t}$$

may be measured by comparing $D^0 \to K^+\pi^-$ and $\bar{D}^0 \to K^-\pi^+$ decays [77], and would (unlike CP-conserving mixing) be a clear signal of new physics. The corresponding asymmetry between D^0 and $\bar{D}^0$ decay rates to K^+K^-, where the D^0 flavor is tagged by the pion from $D^{*+} \to D^0\pi^+$, allows an especially clean measurement since the final state is identical in both cases, and is only singly Cabibbo suppressed. The analysis of this mode is similar to that used for time dependent CP violation in B decay.

There are several classes of rare D decays where the large data samples available at high luminosity will allow improved measurements. Two body decay modes such as $D^0 \to \gamma\gamma, \mu^+\mu^-$ and $\mu^\pm e^\mp$ are strongly suppressed in the Standard Model: expectations are 10^{-8} for $D^0 \to \gamma\gamma$, 10^{-13} for $D^0 \to \mu^+\mu^-$ and 0 for $D^0 \to \mu e$. In new physics scenarios, the rates can be orders of magnitude larger [78]. For example, in both R-parity violating and leptoquark models, the branching fraction for $D^0 \to \mu^+\mu^-$ can be as large as 3×10^{-6} while that for $D^0 \to \mu^\pm e^\mp$ could be 5×10^{-7}. The current experimental bounds for $D^0 \to \mu^+\mu^-$ and $D^0 \to \mu^\pm e^\mp$ are 3.3×10^{-6} and 8.1×10^{-6}, respectively. For 3-body final states such as $\rho\ell^+\ell^-$, where SM expectations are similar, orders of magnitude enhancements are expected at low $\ell^+\ell^-$ invariant masses in some new physics models. In the case of radiative decays such as $D^0 \to K^*\gamma, \rho\gamma$, which are long-distance dominated, measurement at Super KEKB could constrain long-distance effects in the corresponding modes in the B sector.

By the time Super KEKB begins taking data, the tau-charm facility at Cornell will also be operating. Although the design luminosity is relatively low ($5 \times 10^{32}\,\mathrm{cm^2 s^{-1}}$), correlated D meson pairs are produced at threshold from the ψ'' resonance. For measurements where kinematic constraints from production at threshold are essential, such as f_D and D absolute branching fractions, the Cornell facility will remain competitive; and a sensitivity to $D^0 - \bar{D}^0$ mixing at the 10^{-4} level is claimed [75]. Super KEKB will have the advantage of precision vertexing for measurement of time-dependent decay distributions—especially important if CP violation is associated with mixing—and very large D meson samples. Other facilities in the world such as ATLAS/CMS/CDF/D0 cannot do charm physics. LHC-B and BTeV may record large charm data samples if they modify their trigger configurations, which are optimized for B physics. However, these experiments cannot efficiently reconstruct final states with neutrals or K_L mesons.

2.5 Advantages of an e^+e^- B-Factory

One of the primary purposes of the KEKB upgrade is to search for new flavor mixing and new sources of CP violation in physics beyond the Standard Model. In the next decade, novel effects from New Physics, such as SUSY, beyond the energy scale of LHC can only be seen at the luminosity frontier by examining all possible kinds of loop and box diagrams. Even if SUSY particle(s) or other exotics are found at the LHC, the role of the luminosity frontier at low energies is not diminished at all. The rich phenomenology of physics beyond the Standard Model allows many possible scenarios which provide different predictions on the FCNC amplitudes. When the new particles are discovered and their properties, such as mass and spin, are identified, we can set much clearer targets and strategy to investigate loop- and box-mediated effects in rare B decays. Since such effects may not be large, one needs a very clean experimental environment. In this regard, the advantage of an e^+e^- collider at the $\Upsilon(4S)$ energy is clear.

What is truly unique about the $B\bar{B}$ pair production at $\Upsilon(4S)$ resonance is that one can reconstruct one of the B mesons and mask it, so that practically an event with a "single" B meson is available. Even if the final state of interest includes one or more neutrinos, reconstruction with reasonable signal purity is expected. Indeed, if there is just one missing neutrino, it can be "reconstructed" by detecting all other charged and neutral particles, and then forming the 3-dimensional missing momentum. The efficiency to fully reconstruct one B meson is expected to be around 0.2%, resulting in $\sim 6 \times 10^6$ "single" B mesons after three years of operation at Super KEKB. Since it is impossible to reconstruct decays including neutrino(s) in hadronic machines, Super KEKB is the only machine that can be used to establish such decays and to explore manifestations of physics beyond the Standard Model. Decay modes in this category include $B \to K^{(*)}\nu\nu$, $B \to \ell\nu$, $B \to \ell\nu\gamma$, and $B \to \pi(\rho)\ell\nu$, where the last mode is used to measure $|V_{ub}|$, which is an indispensable piece in a comprehensive study of the unitarity triangle.

For final states including γ's and π^0's the e^+e^- environment also has a clear advantage. Examples of the modes we consider are $B^0 \to \pi^0\pi^0$ (needed to examine penguin pollution in $B^0 \to \pi^+\pi^-$), $b \to s\gamma$, $B \to \eta' K_S(\eta' \to \pi^+\pi^-\eta, \rho\gamma)$ (search for new CP-violating phase), and so on.

Finally, even in the case the final state has a distinct signature, it is very challenging to reconstruct rare decays in an inclusive manner at hadron colliders. For example, although the differential and total decay rates of inclusive $b \to s\ell^+\ell^-$ are of great theoretical interest, studies at hadron machines are questionable.

Table 2.1 summarizes the experimental sensitivities expected at an integrated luminosity of 3 ab^{-1} (=3,000 fb^{-1}), which corresponds to three years of data taking at Super KEKB. Fig. 2.5 also shows the expected errors of the time-dependent CP asymmetries for promising FCNC modes and other "reference" modes that provide clean measurements of $\sin 2\phi_1$. As shown in the figure, the decay mode, such as $\eta' K_S$, which is dominated by the loop diagram with a $b \to s$ transition, can be explored down to the precision of 0.1 or less at Super KEKB. Since the ambiguity coming from hadronic uncertainty is estimated to be less than 10%, we can examine the possibility that the $b \to s$ transition contains the new CP-violating phase down to the limit of QCD; *i*.e. a thorough search will be realized with Super KEKB. As a reference, the table also shows the expected sensitivities at LHC.

It should be noted that sensitivities to direct CP violations in some decay modes,

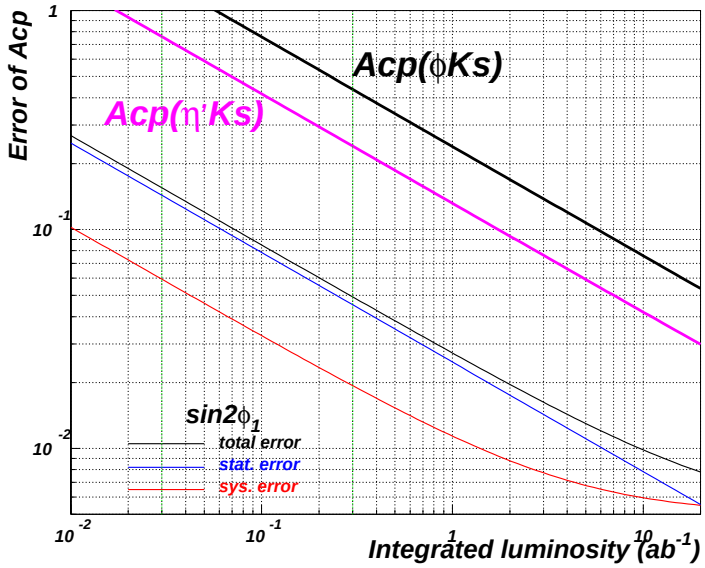

Figure 2.8: Expected errors of CP asymmetries for ϕK_S and $\eta' K_S$ as a function of the integrated luminosity. As a reference, the expected $\sin 2\phi_1$ error, obtained with $J/\psi K_S$ and some other modes which are free from penguin contributions, are also shown.

such as $B \to DK$, are expected to be a few % level, while keeping the systematic errors smaller. Although we need to know the final-state phase differences to extract parameters related to new physics from the measured values of direct CP violation, it is important to detect all varieties of CP violation at Super KEKB.

Table 2.2 is a list of the expected precision of the V_{ub} and ϕ_3 measurements at KEKB/Belle, Super KEKB and the experiments at LHC.

In summary, we can construct a strong physics case for Super KEKB, an e^+e^- collider at $\Upsilon(4S)$ with a luminosity of $10^{35}\mathrm{cm}^{-2}\mathrm{s}^{-1}$. We should utilize the unique feature of the machine, namely the capability to reconstruct neutral particles, such as γ, π^0 and even neutrinos.

Table 2.1: Summary of the estimated precision of CP-violating amplitudes in the proper-time distributions at KEKB/Belle, Super KEKB and planned experiments at LHC. The column labeled by "NP−SM" is the maximum deviation from the SM prediction due to an effect of New Physics (NP). Items marked with "×" cannot be measured at the experiment in question. No information is available for the blank entries.

Decay mode	Theory		KEKB	Super KEKB	LHC		
	SM	NP−SM	(0.3ab^{-1})	(3ab^{-1})	LHCb	ATLAS	CMS
$J/\psi K_S$ etc.	$\sin 2\phi_1$	~ 0.1	0.049	0.016	0.014	0.021	0.025
ϕK_S	$\sin 2\phi_1$	~ 1	0.44	0.14			
$\eta' K_S$	$\sin 2\phi_1$	~ 1	0.24	0.076			
$\pi^+\pi^-$	$\sin 2\phi_2^{eff}$	–	0.19	0.060	0.056	0.10	0.17
$\pi^0\pi^0$ etc.	$\phi_2 - \phi_2^{eff}$	–	20°	7°	×	×	×
$D^*\pi$	$\sin(2\phi_1+\phi_3)$	–	0.24	0.077			
$K_1\gamma$	$\sim m_s/m_b$	~ 0.6	0.77	0.24	×	×	×
$\rho\gamma + \omega\gamma$	$\sim m_d/m_b$	~ 0.6	0.42	0.13	×	×	×

Table 2.2: Summary of the estimated precision of V_{ub} and ϕ_3 at KEKB/Belle, Super KEKB and the experiments at LHC. Items marked with "×" cannot be measured at the experiment in question, while no information is available for the blank entries.

Decay mode	Parameter	KEKB	Super KEKB	LHC		
		(0.3ab^{-1})	(3ab^{-1})	LHCb	ATLAS	CMS
DK	ϕ_3	14°	5°	19°		
$\pi(\rho)\ell\nu$	$\lvert V_{ub}\rvert$	4.3%	1.4%	×	×	×
inclusive lepton	$\lvert V_{ub}\rvert$	2.6%	0.8%	×	×	×

Chapter 3

Upgrade of the KEKB Collider

3.1 Machine Parameters

Super KEKB is an upgrade to the KEKB machine. The target luminosity is 10^{35} cm^{-2}s^{-1}, which is ten-times higher than the design of KEKB[79]. To achieve 10^{35} cm^{-2}s^{-1} luminosity, we propose that the vertical beta function at the interaction point (IP), β_y^*, be 3 mm, that the bunch length (σ_z), also be 3 mm in order to reduce the hour-glass effect, and that the beam currents be 10 A for LER and 3 A for HER. In order to squeeze β_y^*, the final focusing quadrupole magnets (QCS) would be moved toward the IP. We would use a 15 mrad half crossing angle at the IP by rearranging the special IR magnets. A comparison of the KEKB and Super KEKB parameters is shown in Table 3.1. The beam-beam tune shift expected at Super KEKB is assumed to be the same as that at KEKB. The number of bunches is also the same as that at KEKB, since we adopt the same RF frequency as that of KEKB, 509 MHz. It is necessary for Super KEKB to employ high emittance optics due to the large bunch current. The emittance is controlled via the dispersion at noninterleaved 2.5π cells. Wigglers are used in the LER to control the emittance in the preliminary plan.

Table 3.1: Comparison between KEKB and Super KEKB. The parameters of KEKB 2001 are the ones achieved in November 2001.

	KEKB 2001		KEKB (design)		Super KEKB	
Ring	LER	HER	LER	HER	LER	HER
Particle type	positron	electron	positron	electron	electron	positron
Beam energy (GeV)	3.5	8.0	3.5	8.0	3.5	8.0
Beam current (A)	1.07	0.76	2.6	1.1	10	3
Beam-beam (ξ_y)	0.047	0.035	0.05		0.03-0.05	
β_y^* (mm)	6.5	7.0	10		3	
Bunch length (mm)	5-6		4		3	
Emittance (nm)	18	24	18		18-54	
Number of bunches	1153		5120		5120	
Luminosity (nb^{-1})	5.17		10		100	

We have observed a vertical beam blow-up in the positron beam, which degrades

the luminosity at KEKB. We believe that the beam blow-up is caused by photoelectron clouds [80], we can reduce the effect with solenoid coils and ante-chambers. Particle energy-exchange, that is electrons in LER and positrons in HER, may also be helpful to reduce the positron beam blow-up. Therefore, an upgrade of the linac injector is needed to accelerate positrons up to 8 GeV and to increase the injection rates to store large beam currents at Super KEKB.

3.2 Vacuum System

The main issues arise from the intense synchrotron radiation (SR) due to the large beam current. We estimate that the maximum temperature of the copper chamber could be about 310° at a power density of 142 W/mm^2 in LER. Therefore, the present single beam chamber made of copper cannot be used downstream of a bending magnet. In order to cure the heating from SR and/or the effect of the photoelectron cloud, an ante-chamber scheme can be used. A schematic view of the ante-chamber is shown in Fig. 3.1. The ante-chamber consists of a beam channel and an SR channel. A narrow, long slot connects those channels to each other. The beam goes through the beam channel and the SR passes through to the SR channel. The SR is absorbed by a photon stop inside the SR channel. The maximum power density at the photon stop is expected to be 580 W/mm^2 in normal incidence for both LER and HER. One way to reduce the power density is to tilt the surface of the photon stop. When we tilt the surface by 4°, the power density is reduced to 40 W/mm^2. The material of the photon stop should have a good mechanical strength at high temperature and be easy to machine and weld. The most promising material is GlidCop, which is dispersion strengthened copper with ultra fine particles of aluminum oxide. The properties of GlidCop are 100 hours rupture strength and a fatigue strength much higher than that of copper at temperatures above 200°. The thermal conductivity is about 80%, almost the same as that of copper. We calculated the temperature and thermal stress for part of the photon stop. The results are that the maximum temperature is 440° and the thermal stress is 230 N/mm^2. The estimated temperature and thermal stress are half of the melting point and the yield strength. A photon stop made of GlidCop can endure over 10^6 thermal cycles. Thus, GlidCop is a candidate for the photon stop material.

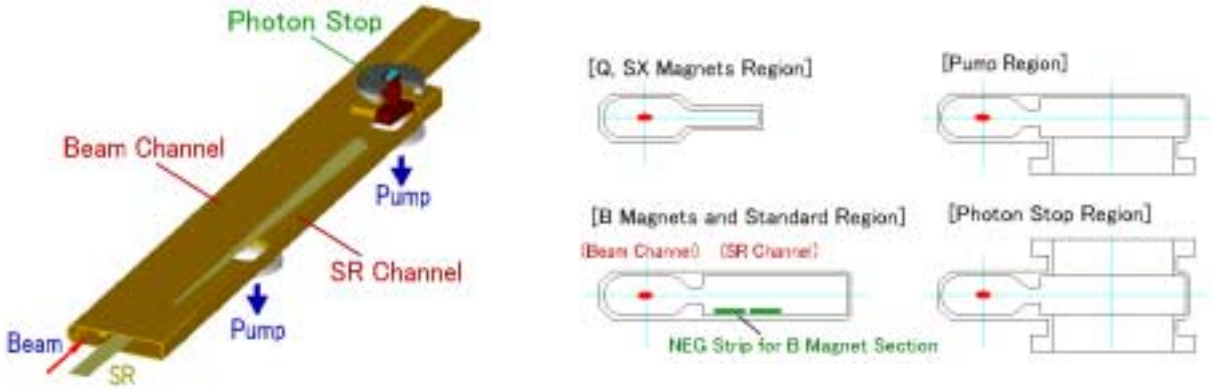

Figure 3.1: Schematic view of the ante-chambers.

Synchrotron light from the positron beam in the HER hits the chamber wall. The

photoelectrons emitted from the wall drift toward the positron beam in the case of a single beam chamber. However, with an ante-chamber, photoelectrons created inside the SR channel do not drift toward the positron beam inside the beam channel. For the ante-chamber scheme for HER, we considered both a photon stop and a saw-tooth surface at the side wall of the SR channel to avoid the effect of photoelectron clouds. The saw-tooth surface is effective to reduce the reflection of SR [81]. If the saw-tooth scheme is possible, we can make the ante-chamber shallow. The cost of a shallow ante-chamber is much lower than that of the normal ante-chamber.

A linear pump speed of 100 ℓ/s/m is required to achieve 3×10^{-7} Pa (3×10^{-9} Torr) at full current and an η of 10^{-6} molecules/photon. The average pump speed just after the NEG (Non Evaporable Getter) activation is 60-70 ℓ/s/m. The pumping speed is restricted by the conductance of the slots at the pumping ports and the spaces between the magnets. The ante-chamber scheme is helpful to achieve the required pumping speed. We can put high-speed pumps, such as ion pumps or titanium sublimation pumps, in the vicinity of the photon stops. The strip type of NEG in the SR channel can be effective. We consider a combination of NEG and ion pumps similar to that in KEKB.

3.3 RF System

One of the major problems caused by the large beam current is the large HOM power deposited in the cavity and other vacuum components. From the point of view of reducing the HOM power, it is preferable that the number of bunches is increased by adopting a higher RF frequency, for example, by a factor of three compared with the RF frequency of KEKB. However, there are many disadvantages with this option; the heat loss per unit area becomes larger, the phase mudulation due to an abort gap increases, and many coupled bunch modes will appear related to the larger detuning. It should also be noted that the cost will be much higher and larger human resources will be needed to develop a completely new RF system with a higher frequency. Also the construction time will be longer in this option.

The present 509 MHz RF system for KEKB employs two types of the damped cavities. One is a normal conducting cavity (NC). It is an accelerator resonantly coupled with an energy storage cavity (ARES). Another is a single-cell superconducting damped cavity (SCC). The RF system with these cavities have been operated very stably with the high current beams in KEKB. They can also be used for Super KEKB, if appropriate improvements and modifications are made to cope with the much higher beam currents. Therefore, we adopt the same RF frequency as that of KEKB, and use as many of the existing RF components as possible for Super KEKB. The improvements should be made not only with the HOM dampers and the input couplers, but also with the high power system and low-leval control system to deal with the heavier beam loading.

The RF parameters are shown in Table 3.2. We will increase the number of ARES cavities from 32 to 40 and SC cavities from 8 to 12. The maximum output power of a klystron is limited to 1.2 MW. The input couplers have been tested up to 1 MW in bench tests and are operated at 200-300 kW in KEKB. The modification to the RF units at Super KEKB is that one 508 MHz 1 MW CW klystron feeds power to one ARES cavity, as opposed to two ARES cavities which is the current scheme at KEKB. The RF unit is one to one for the SC cavities. Therefore, the total number of RF units increases from 24

to 52, including the klystrons, power supplies, high power system and control system.

Table 3.2: RF parameters for Super KEKB.

	LER	HER	
Beam current (A)	10	3	
Energy loss (MeW)	1.6	3.5	
Loss factor (V/pC)	40	40	
Total RF voltage (MV)	15	20	
Synchrotron tune	0.02	0.02	
Radiation loss power (MW)	16	10.5	
Parasitic loss power (MW)	8	1	
Total beam power (MW)	24	11.5	
Cavity type	ARES	ARES	SCC
No. of cavities	30	10	12
Voltage/cavity (MV)	0.5	0.5	1.3
Input coupling	6.33	5.0	-
Loaded-Q value (10^4)	1.5	1.83	4.0
Beam power/cavity (kW)	800	600	460
Wall loss/cavity (kW)	150	150	-
Klystron power (kW)	1000	800	480
No. of klystrons	30	10	12
Total AC plug power (MW)	50	13	9
Detuning frequency (kHz)	75	21	55
Growth rate of -1 mode (s^{-1})	14400	375	
Growth rate of -2 mode (s^{-1})	580	24	
$\Delta\phi$ for 1 μsec gap	27.4°	-	

Table 3.3 shows the HOM power in each cavity estimated at Super KEKB compared with that of KEKB and bench tests. R&D is necessary for the HOM dampers to satisfy the requirements. In addition, the loss factor should be reduced at the dampers and tapers connected to the vacuum chamber. For instance, the diameter of the beam chamber on both sides of the SC cavity is increased from 150 mm to 220 mm to reduce the loss factor of the taper region. The fundamental mode power leaked to the damper is estimated to be 40 kW at the coupling cavity of ARES due to the large beam-loading. The damper structure and the dummy load should be much improved.

Potential problems cannot be cured by the ARES and SC cavities alone for Super KEKB. There are two problems concerning the fundamental mode. One is the longitudinal coupled-bunch instability caused by the large detuning of the cavities. The detuning frequency is 75 kHz in LER, which is the same order as the revolution frequency. The growth rate is 14,400 s^{-1} for the -1 mode and 580 s^{-1} for the -2 mode, respectively. These instabilities should be cured by a feedback system using a comb filter that reduces the impedance at the upper synchrotron sidebands of the revolution harmonics. We have developed a feedback system for the -1 mode, and successful results have been obtained in a bench test. However, the feedback system has to be improved to obtain a 30 dB reduction and to treat multiple modes for Super KEKB. The second is the phase

Table 3.3: HOM power in the cavities together with fundamental power to the coupling cavity of the ARES.

	KEKB 2001	bench-test	Super KEKB
SCC HOM damper (kW/cavity)	7.5	12	30
ARES HOM damper (kW/cavity)	2	26	80
ARES damper at coupling cavity (kW/cavity)	3	20	40

modulation along a bunch train due to the large beam abort gap. The longitudinal beam position is shifted bunch by bunch because of the transient beam-loading at the gap. The phase modulation is roughly proportional to the gap length. If we assume the same gap length to be the same as that of KEKB (1μsec), the phase modulation will be 27.4° for Super KEKB. This is unacceptable. The gap length must be reduced at least by a factor of five to reduce the phase modulation. The gap length is presently determined by the rise time of the beam abort kicker. We need to improve the abort kicker to make the gap length short and to confirm that the beam instabilities can be cured for the short gap length.

3.4 IR Design

The final focusing quadrupole magnets (QCS) should be moved toward the IP in order to squeeze the vertical beta function at the IP. We consider a large horizontal crossing angle and introduce a crab cavity system with special magnets in the IR. We have experiences with small crossing angle, and have successfully operated rings at KEKB. Therefore, the large crossing angle scheme is an advanced strategy. Although the horizontal beta function at the IP is usually determined by the *optimum* x-y coupling condition, we assume that the horizontal beta function is 15 cm at the IP, the x-y coupling is 2%, and the horizontal emittance is 54 nm. The horizontal beta function at the IP is related to the physical aperture in the IR and the horizontal emittance is determined by the assumed beam-beam parameter of 0.05 and the number of bunches (5,120).

We estimated the geometrical loss of the luminosity due to the crossing angle without crab cavities. There is a geometrical loss even if the crossing angle is set to be zero, which is the hour-glass effect due to the finite bunch length. In order to extract the loss due to the crossing angle, we take the ratio of the luminosity to the zero crossing angle. The luminosity reduction as a function of half crossing angle is shown in Fig. 3.2. We consider the 15 mrad half crossing angle for the preliminary design of Super KEKB.

To conserve the detector region and to move both QCS's toward the IP for the IR layout, we make the compensation solenoids (ECS) overlaid on the QCS in the longitudinal direction. The distance between the left QCS and the IP can change from 1.6 m to 1.02 m and from 1.94 m to 1.2 m for the right QCS with this modification. The field gradient of 37 T/m at the excitation current of 3 kA can be obtained, which corresponds to a field gradient that is a factor of 1.9 higher than that of KEKB.

We estimate the physical aperture of the components at the IP from the conditions of the injection beam. Fig.3.3 shows that the acceptance depends on the horizontal beta

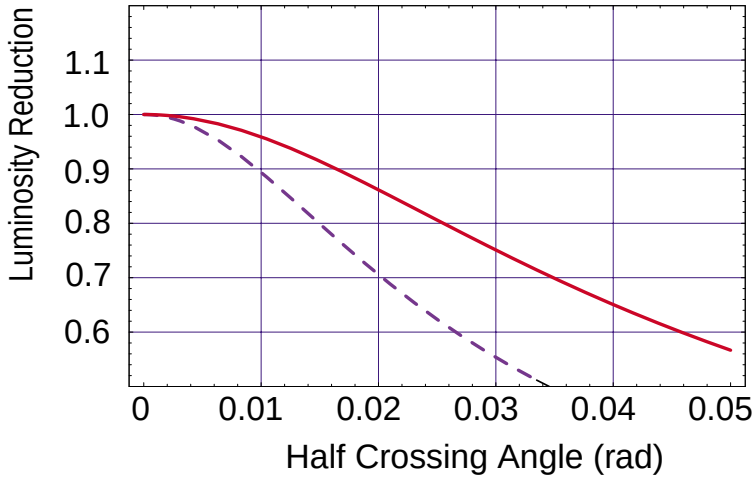

Figure 3.2: Luminosity reduction as a function of half crossing angle. Solid line shows Super KEKB and dashed line for the KEKB design.

function and the emittance. The emittance of the injector beam and injection errors are considered for the required acceptance. Since the required acceptance is insensitive above 100 m of the horizontal beta function at the injection point, we choose 90.4 m, the same as at KEKB. The emittance of the injector beam is rather sensitive to the acceptance and HER is more severe than LER because of the higher beta functions at the IP and the large emittance from the injected positron beam for Super KEKB. The horizontal emittance of the injected beam is 3.3×10^{-7} m for 3.5 GeV energy at the KEKB injector. We assume 1.4×10^{-7} m, which is the same emittance as the present injector, since the beam energy is 8 GeV (HER) for the positron beam at Super KEKB. The required acceptance is 5.6 μm in the horizontal direction from the above condition. The required acceptance in the vertical direction is determined by the vertical emittance and the injection error of the injector. We also assume that the vertical emittance of the injector beam is the same as the horizontal and the injection error is calculated with 2% x-y coupling. The required acceptance is 0.7 μm in the vertical direction.

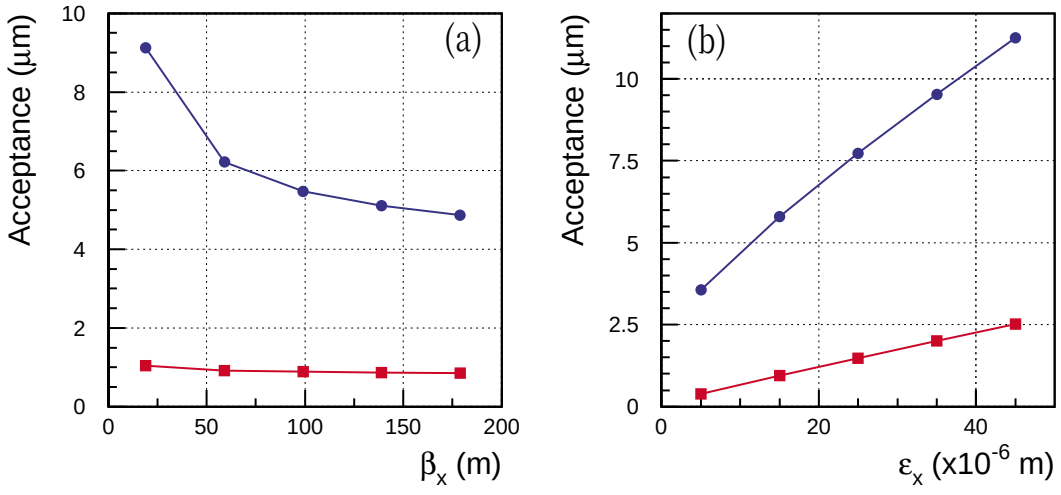

Figure 3.3: Required acceptance as a function of beta function (a) and emittance (b). The circular symbols show the horizontal case and square symbols show the vertical case.

It is necessary to maintain good field quality over a wide region, because a low beta function at the IP is required. The requirement of acceptance for the IR special magnets is very severe in the magnet design at Super KEKB. The specifications for the magnets are listed in Table 3.4. The required areas occupied by the electron and positron beams for QC1RH and QC2RL are shown in Fig. 3.4. We have developed six normal conducting magnets specially designed for the IR at KEKB. One of those magnets is a half-quadrupole magnet and the others are asymmetrical full-quadrupole magnets in which a field-free space is embedded for the beam of the other ring. However, we plan to design all of the six special magnets as asymmetrical full-quadrupole magnets for Super KEKB, since we realize that it is not easy to make a half-quadrupole magnet cover a wide region with good field quality. The design work of the IR special magnets is in progress.

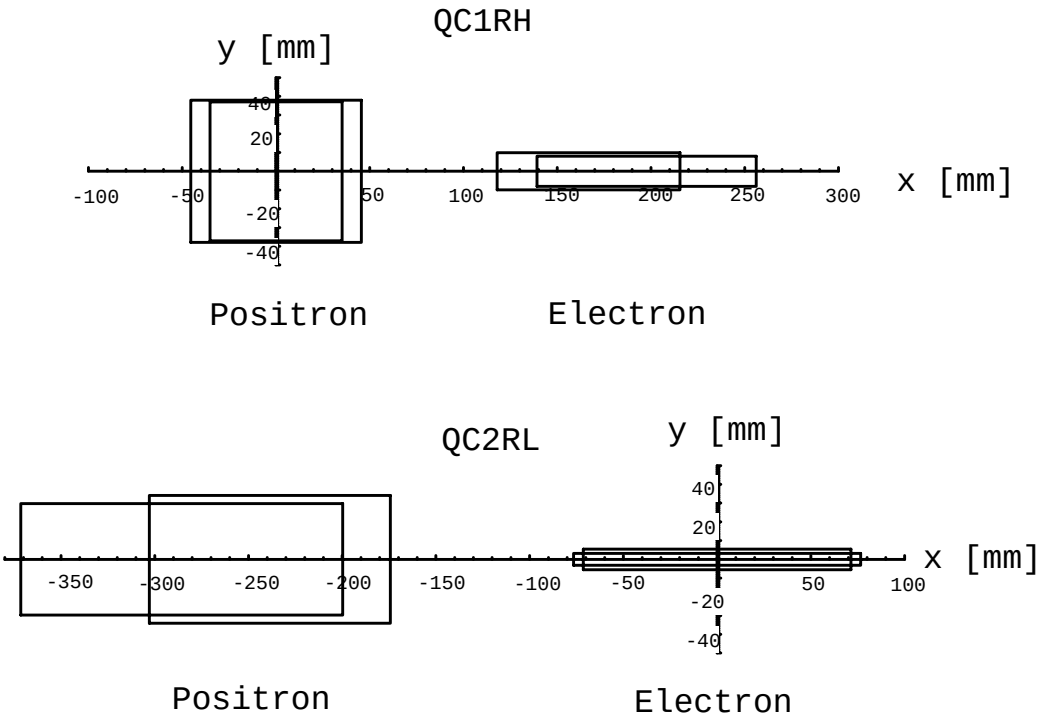

Figure 3.4: Beam positions and beam envelopes during injection at the edge of QC1RH(top) and QC2RL(bottom).

3.5 Beam Instabilities

Ions are produced when the beam ionizes residual gas. The ions that have positive charge can be trapped by the attractive electric force of the electron beam. We usually make a gap that is a series of the empty RF buckets in the bunch train to avoid ion trapping. The gap at KEKB is about 10 μsec, that is 10% of all RF buckets. However, the gap at Super KEKB should be, as short as possible to reduce the modulation of the longitudinal bunch positions due to the transient beam-loading. We estimate the effect of ion trapping for the 2% gap of the total RF buckets with a linear theory. Fig. 3.5 shows the trace of the transfer matrix, M, as a function of the beam current at Super KEKB compared with the case of KEKB. CO is assumed as the ion. Ion trapping can occur if the value

Table 3.4: Specifications of aperture for the IR quadrupole magnets.

		QC1LH	QC2LH	QC1RH	QC2RH	QC2LL	QC2RL
Entrance (e^+)	H (mm)	35.3	103.6	35.2	101.0	53.1	85.9
	V (mm)	30.4	22.8	37.9	27.3	27.2	29.7
Exit (e^+)	H (mm)	26.5	86.7	45.4	106.2	65.0	64.3
	V (mm)	29.1	23.1	38.7	26.6	25.6	34.1
Entrance (e^-)	H (mm)	46.1	45.8	48.8	73.2	60.0	76.6
	V (mm)	7.3	4.0	10.1	1.9	4.2	3.2
Exit (e^-)	H (mm)	36.9	56.9	58.5	70.3	63.0	71.4
	V (mm)	9.2	0.5	8.2	0.9	2.6	5.5
Beam	entrance (mm)	219.2	556.5	166.7	318.4	285.2	285.6
separation	exit (mm)	175.2	409.9	197.2	346.5	329.2	238.6
Field gradient	(T/m)	13.2	11.7	11.7	10.0	6.1	2.9
Pole length	(mm)	0.6	2.0	0.6	0.6	0.6	1.0

of | Trace$(M)/2$ | is less than one [83]. We find that the value of | Trace$(M)/2$ | is much larger than one for both KEKB and Super KEKB and the same order of magnitude. Therefore, ion trapping will not be a serious problem for the 2% gap at Super KEKB.

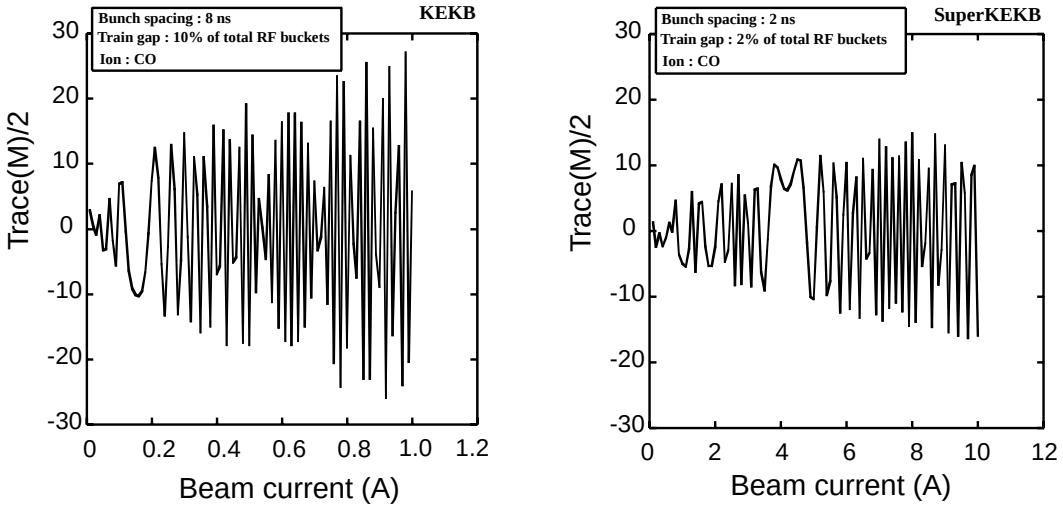

Figure 3.5: Trace of M as a function of the beam current for KEKB(left) and Super KEKB(right).

Even if conventional ion trapping does not occur, ions can be trapped in a single passage of the beam and cause an instability. This phenomenon is called the *fast ion instability*. We estimate the effect of the fast ion instability with Yokoya's formula. The amplitude growth factor, G, of the unstable mode is given by

$$G = \left|\frac{a_n}{a_0}\right| \simeq 1 + \frac{1}{\Gamma} e^{\sqrt{\Gamma}}, \tag{3.1}$$

$$\Gamma = \sqrt{\frac{2m_e}{M_{ion}}}\frac{\beta_y\sqrt{L}}{\gamma}n_g\cdot\sigma_i\left[\frac{r_eN_b}{\Sigma_x\Sigma_y}\right]^{2/3}sn^2, \tag{3.2}$$

where L is the bunch spacing, n_g is the gas density, σ_i is the ionization cross section, $\Sigma_{x,y}$ is the quadratics sum of the beam size and the ion size. The amplitude growth factor for the 500-th bunch as a function of the number of turns is shown in Fig.3.6. For Super KEKB, the initial amplitude grows by 10,000 times in 50 turns, which is the damping time of the present bunch-by-bunch feedback system.

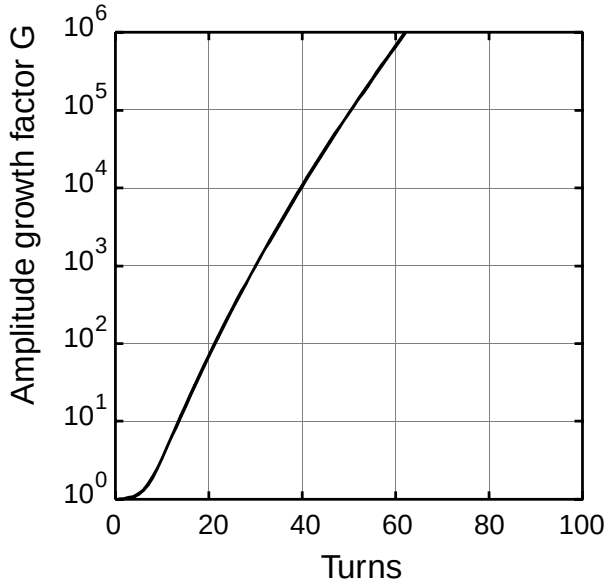

Figure 3.6: Amplitude growth factor of the fast ion instability in Super KEKB as a function of turns. The condition is a beam energy of 3.5 GeV, a bunch current of 2 mA, a CO partial pressure is 1.5×10^{-7} Pa, and a bunch spacing of 0.6 m.

When synchrotron light emitted from the positron beam hits the vacuum chamber wall, photoelectrons are produced and attracted by the electric force of the positron beam. These electrons form a cloud and can cause a coupled-bunch instability and a single-bunch instability.

The growth rate of the coupled-bunch instability due to the photoelectron cloud is given by the imaginary part of the coherent frequency of the instability. The number of emitted photons in one revolution is expressed by

$$N_{e\gamma} = \eta\cdot N_\gamma\cdot N_b, \tag{3.3}$$

where η is the quantum efficiency and N_γ is the number of photons emitted by a positron in one revolution. Since η is proportional to the inverse of the photon energy, the growth rate can be written as

$$g \propto \frac{N_\gamma}{\epsilon_c\gamma}, \tag{3.4}$$

where ϵ_c is the critical energy, and γ is the Lorentz factor. Table 3.5 shows the parameters at KEKB and Super KEKB. Thus, we obtain the ratio of the growth rate at Super KEKB

to KEKB to be

$$\frac{g(SuperKEKB)}{g(KEKB)} = \frac{6}{11}\frac{3.5}{8}\frac{9.4}{4.1} \simeq 0.5. \tag{3.5}$$

Table 3.5: Parameters of the beam energy, number of photons emitted from the beam, and critical energy for KEKB and Super KEKB.

	Energy (GeV)	N_γ	ϵ_c (keV)
KEKB	3.5	4.1	6
Super KEKB	8.0	9.4	11

If the density of the photoelectron cloud reaches the neutralization density, as shown in a recent simulation[80], the number of emitted photons in one revolution, $N_{e\gamma}$, in Eq. (3.3) is replaced by the number of electrons at the neutralization level, as follows:

$$N_{en} = k \cdot \frac{C}{s_b} \cdot N_b, \tag{3.6}$$

where k is the neutralization factor, C is the circumference of the ring and s_b is the distance between adjacent bunches. Therefore, the growth rate is proportional to the inverse of the Lorentz factor, and one can obtain

$$\frac{g(SuperKEKB)}{g(KEKB)} = \frac{3.5}{8} \simeq 0.4. \tag{3.7}$$

The growth rate will be half of that of KEKB in either case.

Blow-up of the transverse beam size has been observed at KEKB and PEP-II. We suggest that a single bunch head-tail instability caused by the photoelectron cloud invokes blow-up. This model was proposed by F.Zimmermann and K. Ohmi [82]. The threshold density of the photoelectron cloud, ρ_c, at which a strong head-tail instability appears agrees with the calculated built-up cloud density at KEKB. From the two-particle model, the threshold density is given by

$$\rho_c \propto \gamma \cdot \nu_\beta \cdot \nu_s, \tag{3.8}$$

where ν_β and ν_s are the betatron and synchrotron tune, respectively. The beam energy of the positron ring will be changed from 3.5 GeV to 8 GeV at Super KEKB. This modification would increase the threshold density, ρ_c, by a factor of 2.3. However, the threshold density also depends on the bunch length. This dependence on the characteristics of the wake with the photoelectron cloud should be calculated, since the bunch length is 3 mm at Super KEKB instead of 5 mm at KEKB.

3.6 Cooling System

The power loss from the magnet system, SR, HOM, and RF system is shown in Table 3.6. The power loss from the magnet system is 10 MW in total, which is the same for KEKB

and Super KEKB. The total power loss at Super KEKB is 83.4 MW, which is three-times larger than at KEKB. If we give up on wigglers in LER, the total power loss becomes 66.5 MW. This number is twice that of KEKB. However, we obtain a simulation result that the luminosity is degraded as the damping time increases. Fig.3.7 shows the luminosity per bunch as a function of the longitudinal damping time of LER. The damping time is 20 msec with wigglers and 40 msec without wigglers. The luminosity is estimated to be degraded by 30% in the case of no wigglers. This is the trade-off of a 17 MW power loss reduction and a 30% luminosity loss. Alternatively, one can choose half of the wigglers to be used at Super KEKB. The cooling system must be upgraded for Super KEKB whether wigglers exist or not.

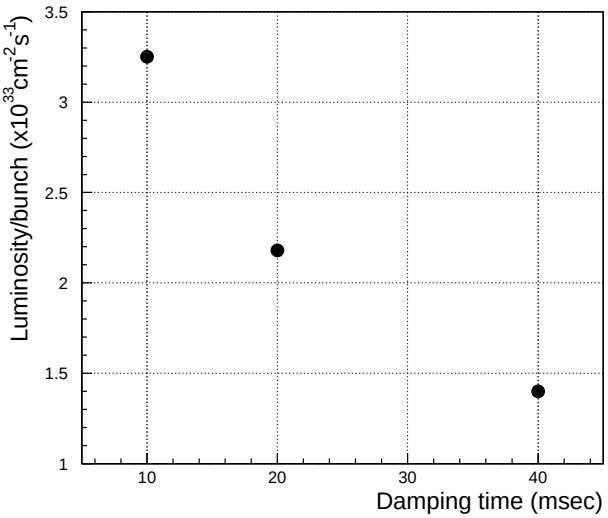

Figure 3.7: Simulation result of the luminosity per bunch as a function of the longitudinal damping time of LER. The bunch current is 0.63 mA for LER and 0.50 mA for HER. β_y^*=0.7 mm, ϵ_x=24 nm, ϵ_y/ϵ_x=2%, σ_z=5.5 mm for LER and β_y^*=0.7 mm, ϵ_x=18 nm, ϵ_y/ϵ_x=1%, σ_z=5.6 mm for HER.

Table 3.6: Comparison of the power loss between KEKB and Super KEKB.

	KEKB 2001	KEKB (design)	Super KEKB	Super KEKB w/o wiggler
Magnet p.s.	3.84			
Magnet	6.35			
SR	4.3	8.0	26.5	18.5
HOM	0.40	0.43	8.7	6.8
RF system	12	16	38	31
Total (MW)	26.9	34.6	83.4	66.5

The present cooling system at KEKB is shown in Table 3.7. Although the total cooling capacity is 84.73 MW, the location, water type, and flow rate that is required for each component should be taken into account. The cooling system is divided into four sections: Fuji, Nikko, Tsukuba, and Oho along the KEKB ring. The upgrade of the RF system

for Super KEKB is concentrated at the Fuji section, and a cooling of 20 MW capacity is necessary, at least. New buildings must be built in the vicinity of Fuji for the additional cooling systems. On the other hand, cooling for the vacuum chamber is needed along the whole ring. For each section, at least 6.6 MW cooling capacity is necessary for the vacuum chamber.

Table 3.7: Cooling capacity at present system.

component	pump	location	water type	flow rate (ℓ/min)	capacity (MW)	requirement (MW)
Klystron		Fuji		3390/2700	4.730	20.0
Magnet P.S	PWP-1	Nikko	pure	2590/1700	3.614	4.0
		Tsukuba	water	3640/3600	5.079	←
		Oho		3590/3300	5.009	5.0
Cavity	PWP-2	Fuji	marine	6300/5000	4.395	6.5
		Oho	blue	6300/2300	6.593	3.0
		Fuji		4020/3800	6.491	←
Magnet	PWP-3	Nikko	pure	3860/4500	5.947	←
		Tsukuba	water	3660/4100	5.737	←
		Oho		3660/4800	5.737	←
		Fuji		1600/2400	1.116	6.6
Vacuum	PWP-5	Nikko	pure	1600/2400	1.116	6.6
		Tsukuba	water	1600/2401	1.116	6.6
		Oho		1600/2402	1.116	6.6
Dummy load		Fuji		6614/7400	6.923	←
RF P.S	CP-1	Nikko	water	4410/5000	4.615	←
Vacuum(2)	CP-3	Tsukuba		7350/7400	7.703	←
		Oho		7350/5700	7.692	←
Total					84.73	

3.7 Injector Linac

The injector Linac must be upgraded for beam injection to a higher luminosity machine, Super KEKB. We have found that the luminosity is degraded by the beam blow-up due to the photoelectron cloud in the positron ring at KEKB. Thus, the exchange of beam energy between electrons and positrons may reduce the effect of beam blow-up, because the interaction between the positron beam and the photoelectrons will be small for the higher beam energy. Consequently, the beam energy of the electrons becomes 3.5 GeV in LER and the positron becomes 8.0 GeV in HER as a result of the energy exchange. Another advantage is the injection time. Because the intensity of the positron beam is usually smaller than that of the electron beam in the injector linac, the positrons should be injected to the lower current ring (HER) that corresponds to the higher energy ring. In order to exchange the beam energy, an energy upgrade of the positron beam line is needed.

A positron target is placed at the middle point of the beam line to obtain a higher energy of the primary electrons and to accelerate the positron beam up to 3.5 GeV at the present KEKB. It is impossible to accelerate the positron beam up to 8 GeV without any modification of the beam line. A simple extension of the beam line cannot be adopted, because of the limitation of the KEK site. We have two energy upgrade schemes for the positron beam. One is a higher field gradient scheme and the other is a recirculation scheme.

We plan to use a C-band accelerating structure instead of the S-band for the higher gradient scheme. The C-band has been developed for the Japanese Linear Collider (JLC) at KEK. The RF frequency of the C-band is 6 GHz and the field gradient is typically 40 MV/m. The iris aperture is acceptable for the large beam emittance of the injector linac when the number of quadrupole magnets is increased to focus the beam. We also consider a damping ring to reduce the emittance. The design of the C-band is based on that of the JLC-C group. The JLC-C group adopts a special structure that is HOM free for a multi-bunch wake field. However, we use an ordinary structure that gives a better shunt impedance, since it is not necessary to use such a structure for Super KEKB.

The acceleration field is calculated by

$$E_0 = \sqrt{2\pi f \frac{r_0 P}{\nu_g Q}}, \tag{3.9}$$

where f is the RF frequency, r_0 is the shunt impedance, P is the klystron power, ν_g is the group velocity, and Q is the quality factor. The parameters of C-band compared with the S-band are shown in Table 3.8. The RF system must be greatly modified to accomodate the C-band structure. The klystron, the SLED cavity and the microwave guide, in particular, must be replaced. Since a power of 100 MW from the klystron is required, we use a pair of 50 MW klystrons. Because the C-band has a twice higher RF frequency, the length of the RF pulse fed into the SLED cavity becomes half compared with that of the S-band. The modification of the pulse modulator would be small because the energy stored in the pulse modulator would be slightly higher. Assuming an acceleration field of 40 MV/m with the C-band, the energy gain per unit would be 308 MeV. When we upgrade 26 units to the C-band out of 30 units, the energy of the positron beam becomes 8.65 GeV at maximum. Therefore, this is enough for an 8 GeV positron beam even if two units are on standby. We consider the following items:

- Design and prototype fabrication of the C-band accelerating structure optimized for the injector linac at Super KEKB
- High-power test of the structure
- Modification of the pulse modulator to drive two klystrons
- Klystron design and prototype fabrication (klystron developed by the JLC-C group will be commercially available. Another possibility is the S-band klystron with a modified output coupler to obtain the C-band output in harmonics generation.)
- SLED design and prototype fabrication
- Beam optics and tracking simulations for the small aperture of the C-band.

- Bunch compressor to obtain a good energy spread

The C-band scheme is straightforward, while the recirculation scheme is complicated. The recirculation scheme includes a damping ring and a positron return line. The positron beam generated at the target is accelerated up to 1 GeV and then injected into the damping ring. The positron beam extracted from the damping ring returns to upstream of the beam line in synchronization to the timing of another RF pulse, and is accelerated with primary electrons from the gun simultaneously. Both positron and primary electron beams are accelerated and then separated using a bending magnet before the target. The primary electron beam hits the target and generates new positrons. The positron beam accelerated with the primary electron beam, goes through a bypass line to the second half of sector 2 and is accelerated up to 8 GeV. Because there is the J-arc, that is a 180° arc between the B and C sectors, two J-arcs are necessary for the electron and positron beams. It is not necessary to modify the RF system and the accelerating structure in the recirculation scheme. However, the beam focusing optics must be compatible with two positron beams with different energies while going through the same accelerator units simultaneously.

Table 3.8: Parameters of the S-band and C-band accelerating structure.

		S-band	C-band (JLC-C)
RF frequency (f)	(MHz)	2856	5712
Shunt impedance (r_0)	(MΩ/m)	55	53
Quality factor (Q)		14100	9950
Group velocity (ν_g)	(c)	0.019	0.035
RF power from klystron	(MW)	41 (4μsec)	100 (2μsec)
Power multiplication		3.4 with SLED	
Accelerating field (E_0)	(MV/m)	21	40

In the upgrade of the injector linac, the increase of the beam intensity is also important for achieving a high integrated luminosity at Super KEKB. We define the *luminosity efficiency* as the ratio of the integrated luminosity to the product of the peak luminosity and run time. Fig. 3.8 shows the luminosity efficiency as a function of the injection rate of LER at Super KEKB. The dependence of the HER injection rate is not very large. The luminosity efficiency of KEKB 2001 is 81% and well optimized. However, the luminosity efficiency at Super KEKB is estimated to be 36% if the beam intensity of the injector linac is not increased. When we assume an injection rate of 15 mA/s for LER and 3 mA/s for HER, the luminosity efficiency goes up to 61%. The injection rates at KEKB are typically 1.5 mA/s for LER and 3 mA/s for HER so far. In order to increase the electron injection rate by a factor of five, we increase the beam intensity from 1 nC to 5 nC per bunch. There is no difficulty in the linac injector, in principle, because an intensity of 10 nC/bunch for the primary electron has been achieved. For the positron beam, we adopt two-bunch acceleration to get a factor of two. The two-bunch acceleration has already been tested and successfully performed. An advantage of the C-band scheme is that it is easier to perform two-bunch acceleration rather than the recirculation scheme. In the case of the recirculation scheme, another way to increase the beam intensity is to introduce

a flux concentrator type of solenoid, as used at SLC/SLAC. When the beam intensity is increased, the emittance will be large. The beam quality will become worse with the C-band scheme if the present energy compressor is used for the 8 GeV positron beam. If the beam quality is problematic, a positron damping ring should be constructed to make a positron beam of good quality. Moreover, if the simultaneous injection of both electrons and positrons is possible, the luminosity efficiency would be greatly improved. There is a feasibility of simultaneous injection for both the C-band scheme and the recirculation scheme.

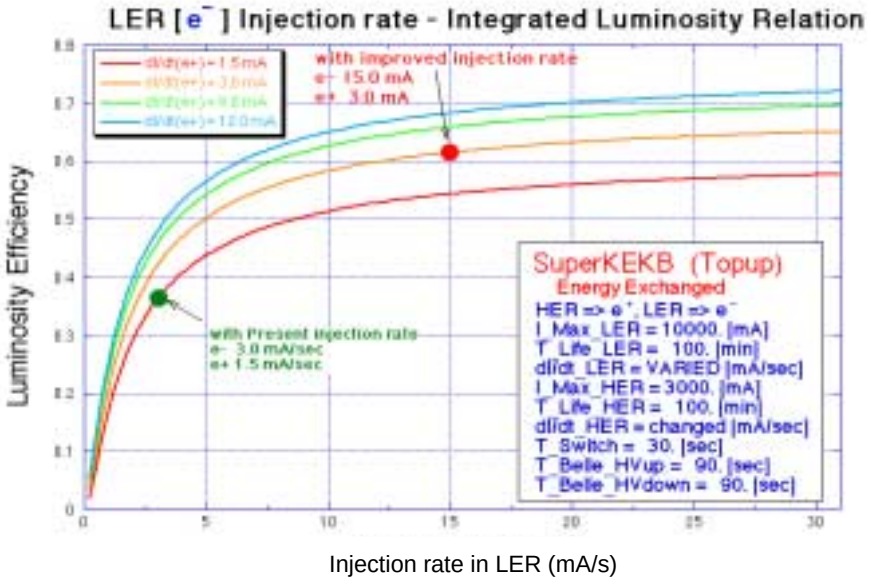

Figure 3.8: Dependence of the luminosity efficiency on the injection rate.

3.8 Strategy toward 10^{35} cm^{-2} s^{-1}

The Super KEKB of luminosity 10^{35} cm^{-2}s^{-1} is not trivial for either the accelerator design or construction. One problem will be the power consumption of Super KEKB is very high. The higher order mode (HOM) losses will reach 8.7 MW due to the short bunch length. In order to reduce the HOM loss, we have to measure the impedance precisely at KEKB and make a precise estimate for Super KEKB. It is necessary for Super KEKB to consider some innovative design of the vacuum chamber, such as bellow-less connections. Another source of power consumption is synchrotron radiation from the wigglers in LER. The effect of radiation damping on the luminosity by the wigglers has not been confirmed experimentally at KEKB. Since the stored beam current will be increased gradually as is done at KEKB, there is no reason to remove the wigglers in the beginning. They will be turned off or weakened as the beam current increases. The present LER chicane to change the path length cannot be adjusted during operation of a physics run. When we remake the chicane so as to adjust the path length easily, a variable wiggler operation is possible during a physics run.

We hope that energy exchange will be helpful for reducing the injection time and the beam blow-up of a positron beam. Before making a decision concering the energy

exchange, two questions must be answered experimentally: (1) Is the electron beam in the LER safe against ions? (2) Is the positron beam in HER safe, especially in the bending magnets and the vacuum chamber? The first question will be answered by an experimental injection of electrons into LER. The second question is hard to answer because we cannot test it until the injector linac is upgraded. The narrow height of the HER vacuum chamber can be problematic for multipacting. Though the predictability is limited, several tests must be done in LER, such as a beam test for a HER-shaped vacuum chamber with a photoelectron cloud monitor in a bending magnet.

Another issue is the necessity of the positron damping ring before injection to the ring. With a smaller beta function at the IP, the injection emittance should be reduced from the present emittance of the injector linac.

The current design parameter is $\beta_y^* = 3$ mm, which is equal to the bunch length. We should investigate the possibility of a smaller beta function, say 2 mm, even though it is below the bunch length. The dynamic aperture would be affected further, but techniques with chromatic octupoles and decapoles may work.

The construction schedule of Super KEKB is given in Fig. 3.9. The R&D and productions of various components will be done in the first four years in parallel with the physics experiment at KEKB. The installation will be done during a one year shutdown in 2006, then the commissioning of Super KEKB will start.

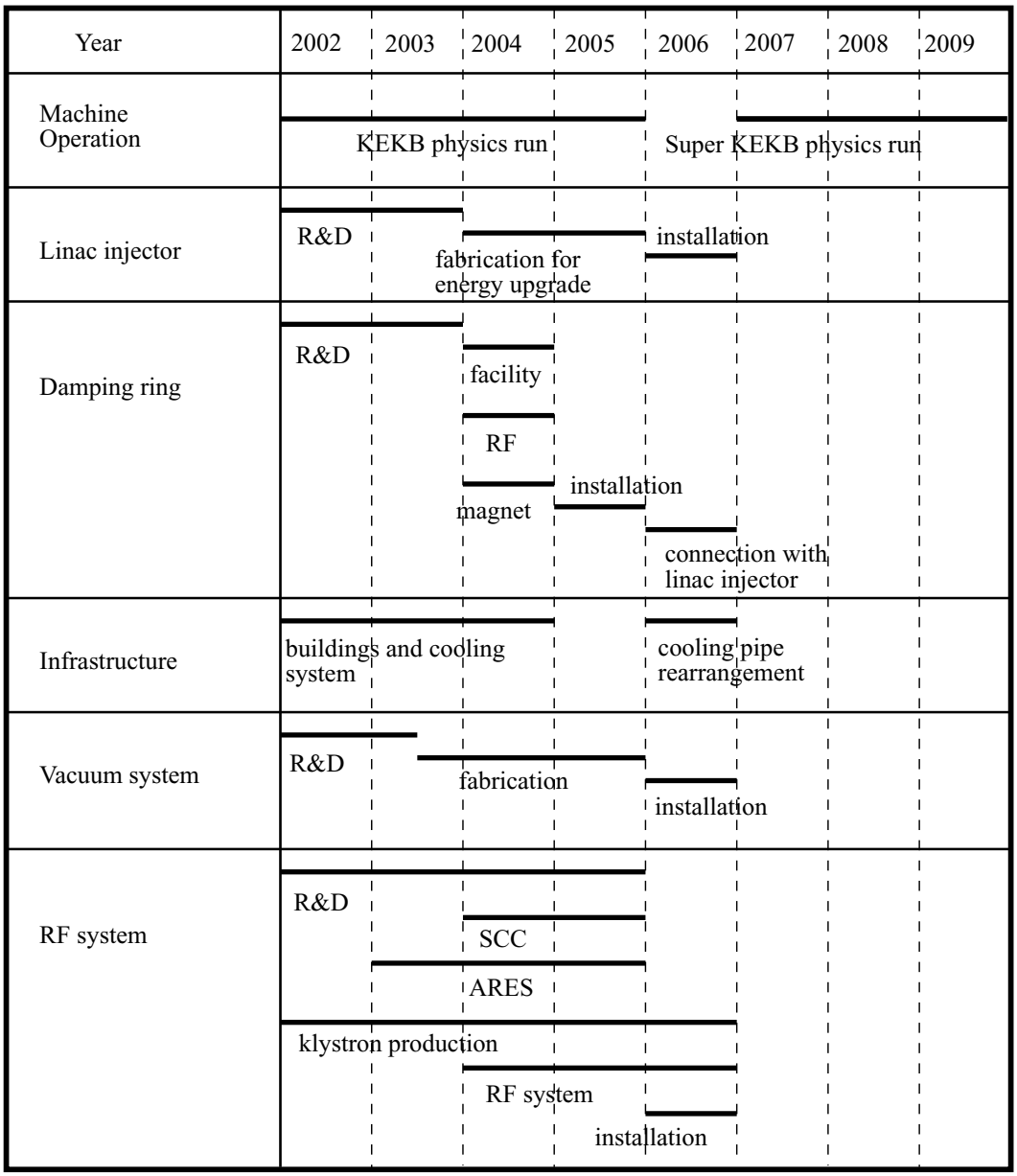

Figure 3.9: Construction schedule of Super KEKB.

Chapter 4

Upgrade of the Belle Detector

The present Belle detector [85] is a general-purpose large solid-angle magnetic spectrometer surrounding the interaction point. It consists of a barrel, as well as forward and rear components.

Precision tracking and vertex measurement are provided by a central drift chamber (CDC) [86] and a silicon vertex detector (SVD) [87]. The CDC is a small-cell cylindrical drift chamber with 50 layers of anode wires filled with a low-Z gas mixture to minimize multiple Coulomb scattering so as to ensure a good momentum resolution, especially for low momentum particles. The SVD consists of three layers of double-sided silicon strip detectors (DSSD) surrounding the beam-pipe, a double-wall beryllium cylinder of 2 cm radius.

For the separation of charged pions and kaons, three systems are employed: the CDC for dE/dx measurements, time-of-flight counters (TOF) [88], and the aerogel Čerenkov counters (ACC) [89]. The CDC provides measurement of the energy loss for charged particles with a resolution of $\sigma(dE/dx)= 6.9\%$. The ACC consists of 1188 aerogel blocks with refractive indices of between 1.01 and 1.03, depending on the polar angle. Electromagnetic calorimetry is performed by a CsI(Tℓ) crystal calorimeter (ECL) [90] consisting of 8736 crystal blocks of 16.1 radiation length (X_0) thick.

The detectors mentioned above are inside a 1.5 Tesla super-conducting solenoid of 1.7 m radius. The outermost spectrometer subsystem is a K_L and muon detector (KLM) [92], which consists of 14 layers of iron absorbers alternating with resistive plate counters (RPC).

All of these detectors show excellent performance at the present KEKB with a luminosity of $5 \times 10^{33}\mathrm{cm}^{-2}\mathrm{s}^{-1}$. When KEKB is upgraded to Super KEKB, however, a major upgrade has to take place with the detector at the same time to take a full advantage of the high luminosity, where a much higher hit rate and radiation dose are expected at all of the detector components. Possible plans of the detector upgrade are described in the following sections.

4.1 Beampipe and Mask System

There are a number of issues that need to be addressed for the detector-machine interface of Super KEKB. It is likely that background caused by lost particles will become a bottle neck of the IR design for Super KEKB. There are a few guidelines that are effective in reducing the particle background: (1) A set of massive masks will be needed near the

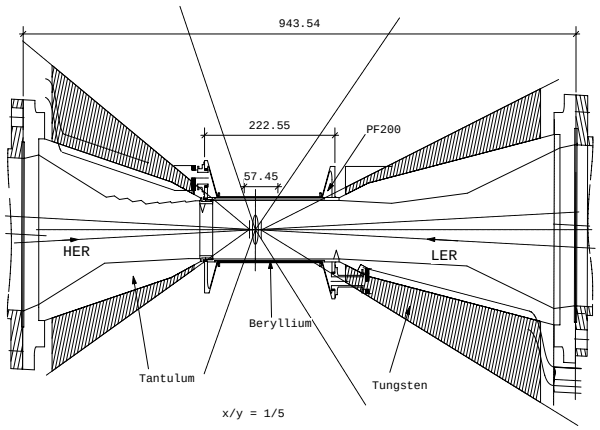

Figure 4.1: Possible r=1 cm IP beampipe design which respects the fiducial region of the extreme forward counter.

(MRad/yr=10^7 s) for (1 nTorr CO, 3 A/10 A)				
	Conservative		Optimistic	
r(b.p.)	1 cm	1.5 cm	1 cm	1.5 cm
HER sum	0.5	0.2	0.2	0.1
LER sum	6.8	0.6	2.3	0.2
Total	7.3	0.8	2.5	0.3

Table 4.1: Expected particle background for Super KEKB. The numbers are for two kinds of extrapolation from a simulation performed for the Belle SVD2.0 upgrade.

IR beampipe. They should have at least about 10 cm of inner surface parallel to the incoming beam (see Figure 4.1) in order not to spray showers into the detector; once a particle is intercepted by a mask, the shower should be absorbed. Such a design becomes difficult as the crossing angle increases, since the length of such a section becomes limited by the beam-stay-clear of the outgoing beams. An integrated design of the support of the vertex detector and the particle mask may make sense. (2) The region upstream of the IR beampipe should be systematically covered by heavy masks. (3) The placement of the movable masks needs to be carefully planned such that the particle loss will occur away from any weak spots, including the IR itself.

Table 4.1 shows the expected particle backgrounds for Super KEKB which are extrapolated from the simulation performed for the Belle SVD2.0 upgrade. Here, we use two kinds of extrapolation: (1) A conservative choice assumes that the background is proportional to the beam current and τ^{-1}, where τ is the lifetime of the beam. (2) An optimistic choice assumes that the background scales with the beam current. If the background scales with the amount of particles lost, then the conservative version should be used. The optimistic case assumes that there will be further improvements in background reduction.

Since vertex detectors are known to survive dose of 10 MRad or more, the radiation dose itself is not a problem. However, the occupancy will be on the order unity for the beampipe radius (r) of 1 cm which indicates that a pixel device will be needed. The r=1.5 cm would be a fall-back design; still, the occupancy will be difficult to handle with a strip detector. This large difference between the two radii is due to the Touschek background, which peaks sharply near zero energy loss as can be seen in Figure 4.2. As a result, the particles hitting a mask at a small radius can spray shower debris into

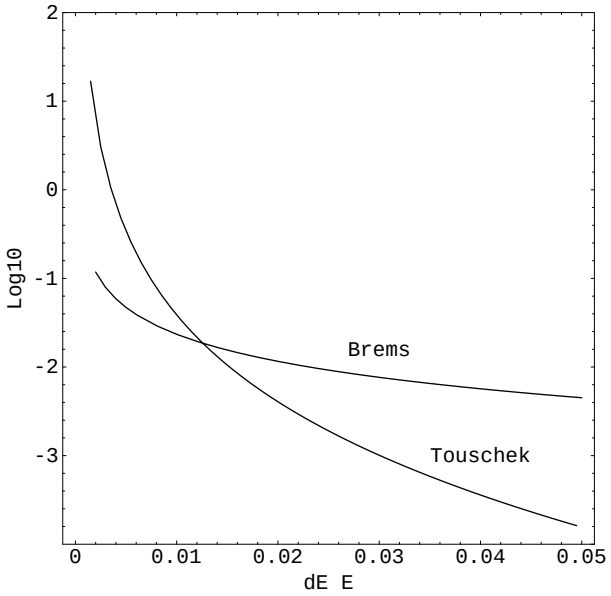

Figure 4.2: Energy-shift spectrum for Bremsstrahlung, which is always an energy loss, and the Touschek effect, where one particle gains energy and the other loses it.

the vertex detector. This can be improved by making the beampipe and the innermost section of the vertex detector with a light material, so that the particles can pass through without making showers. A preliminary study showed that such a design can reduce the background by about a factor of two.

There are at least three sources of SR background that we should consider: the incoming HER, the incoming LER, and the outgoing HER. The synchrotron radiation from the incoming HER can be significantly reduced by using a sawtooth design for the outer-x wall of the beampipe and by a SR mask just upstream of the Beryllium section of the beampipe, as shown in Figure 4.1. Furthermore, the inside surface of the beampipe should be coated with a heavy metal, such as gold, to suppress X-rays passing through it. Simulation studies showed that a gold coating of 10 μm thickness can reduce the dose by roughly two orders of magnitude. The expected dose depends strongly on the orbit offset at the final focusing quadrupole, QC1. If there is no offset, the expected dose is 5 kRad a year, which increases to 670 kRad if the y offset is 3mm. Either the offset should be limited, or a reliable SR projecting program needs to be developed which can issue an alarm when the orbit is such that a large SR background may result.

The incoming LER beam has much lower critical energies and in general does not cause severe problems. Probably, no SR mask will be needed on the LER side.

	Super KEKB
I: (A) (LER/HER)	10/3
$b_{\rm sp}$:bunch sep. (m)	0.6
σ_z: bunch length (mm)	3
δ: skin depth (μm)	0.7
$P_{\rm image}$ (kW) (LER/HER)	0.24/0.02
$P_{\rm tot}$ (kW)	0.78
ΔT (K), outer Be	0.5
ΔT (K), inner Be	2.0

Table 4.2: Beam parameters and the expected temperature rise (ΔT) of the Be beampipe.

The outgoing HER passes the closest IR quad (QCSR) with a 4cm offset, which leads to 100 kW of SR radiation with a critical energy of 40 keV. The backscattering from the dump, which is currently located 8 m away, can cause significant background at IR. If there is no mask, about 60 kRad/yr is expected. With a mask, it will be small, but then a HOM resonance needs to be avoided by judicious adjustment of the dimensions, which is in principle possible, but the required accuracy is close to the engineering limit.

The heating of a beampipe due to image current is given by

$$P_{\rm image}(W) = \frac{\Gamma(\frac{3}{4})}{4\sqrt{2}\pi^2}\sqrt{\frac{c\,\mu}{\sigma}}\,\frac{I^2 b_{sp}}{\sigma_z^{3/2}}\,\frac{L}{r},$$

where the beampipe length (L) and radius (r), the bunch spacing (b_{sp}), and the bunch length (σ_z) are in m, σ is the conductivity of the surface material (unit is $1/\Omega m$), and μ is the permeability ($4\pi \times 10^7$ N/A^2 for non-permeable metals). The heating due to HOM loss is not easy to estimate; we will, however, assume that it is twice the image current heating. This assumption is consistent with measurements of the current beampipe.

The inner surface of the IR beampipe should be coated with a highly conductive material to reduce the heating. The gold SR coating mentioned earlier can also act as such a coating. Because the skin depth at the KEKB RF frequency is on the order of 1 μm, a 10 μm thick coating would be enough. The expected amount of heating of the IR beampipe is 0.78 kW total. Such heat is difficult to handle with a gas cooling, and therefore liquid cooling would be a necessity. In particular, water seems to be by far the best coolant with its high heat conductivity, heat capacity, and a good viscosity. The water, however, should be kept free of contaminants that corrode beryllium, such as chlorides and sulfides. The inside of the cooling channel should also be treated, for example, by a single-component epoxy, such as BR127. The cooling channel is assumed to be a 0.5 mm gap between two beryllium cylinders. The length of the beampipe is taken to be 10 cm. The pressure needed for 11 ℓ/s of water to flow through the channel is 9.4 psi where the flow is a well within the turbulent range. The result of the cooling analysis is shown in Table 4.2. For Super KEKB, the temperature rise is not severe with only 2 degrees C of temperature rise for the inner Beryllium cylinder, and the coolant flow can be reduced from 11 ℓ/s.

4.2 Vertex Detector

The vertex detector (VXD) at the high-luminosity asymmetric e^+e^- collider will play an essential role in a wide range of time-dependent physics analyses that include measurements of mixing-induced CP violation, such as $\sin 2\phi_1$, $\sin 2\phi_2$ and $\sin(2\phi_1 + \phi_3)$, searches for a new source of CP violation in penguin decays, and a search for $D - \overline{D}$ mixing. It is also expected to reduce the background in the measurements of rare decays, especially in analyses which require the full-reconstruction technique, by providing a better vertex resolution than what has been achieved so far at Belle in order to distinguish tracks in one B decay from the other with higher efficiencies.

The silicon vertex detector (SVD) being used at Belle consists of three concentric cylindrical layers of double-sided silicon strip detectors (DSSD's). The radii of the three layers are 30, 45 and 60 mm around the beampipe of 2 cm radius. The signal-to-noise ratio has been measured to be better than 17. The effective strip pitch is 25 μm on the $r\phi$ side and 84 μm for the z side. The angular coverage is $23^\circ < \theta < 140^\circ$, which corresponds to 86% of the full solid angle, where θ is the angle from the beam axis, which is defined as z-axis. With this configuration we obtain a proper-time resolution of about 1.5ps (rms), and an overall vertex reconstruction efficiency of 86%. In the summer of 2002, we plan to install a new SVD with a 1.5 cm radius beampipe to further improve the vertex resolution.

At the present luminosity, which is below $10^{34}\mathrm{cm}^{-2}\mathrm{s}^{-1}$, the performance of the SVD is good enough for a time-dependent analysis, although better resolution is desirable for background rejection in a rare-decay analysis. At a luminosity of $10^{35}\mathrm{cm}^{-2}\mathrm{s}^{-1}$, however, the present SVD will not work because the SVD occupancy becomes untolerably high. At present, the average SVD occupancy in the innermost layer is about $3 \sim 5\%$. Assuming that the occupancy is proportional to the annual dose, we can guess the expected occupancy at Super KEKB in the case that we use silicon strip detectors with the same pitch, but with the length scaled to be half, since we would like to improve the resolution by reducing the radius of the beampipe. The expected occupancy is obtained to be 274% for an area of $50\mu\mathrm{m} \times 2.7\mathrm{cm}$ ($= 84\mu\mathrm{m} \times 640$ / 2). In order to reduce the occupancy to a tolerable level, therefore, we definitely need to introduce a pixel detector. Taking into account the large uncertainty in this calculation, we should choose the pixel size in such a way that the expected occupancy becomes around 1% so that we would have a sufficient margin. Then, the required pixel size is approximately 50 μm $\times$ 100 μm.

The requirements for the pixel vertex detector are summarized as follows:

- The pixel size should be around 50 μm $\times$ 100 μm,
- The detector should be thinner than 300μm to minimize multiple Coulomb scattering,
- As explained above, the occupancy should be around 1%,
- The annual radiation dose, based on simulation tools which can reproduce the present dose with a reasonable precision, could reach 7.3MRad. Therefore the pixel detector should be radiation-hard,
- The signal-to-noise ratio should exceed 20, and the common-mode noise should be less than 500 e^-, and

- The readout speed should be fast enough to satisfy the requirements from the trigger and DAQ.

As for the available technologies to realize a pixel vertex detector, we think that there are three candidates:

- Hybrid pixel detector.
  The LHC experiments (ATLAS and CMS) will use this technique. Thus, this technology will be throughly tested by many groups. The radiation hardness is also expected to be guaranteed. One problem is the thickness of the detector. This is not a major limitation at very high energy, but at B factories it certainly creates a larger amount of multiple scattering, which degrades the vertex resolution.

- CCD pixel detector.
  The success of the SLD experiment has proven that this technology is mature enough to be used in collider experiments. However, the readout speed and the radiation tolerance are problematic for this technology at a high-luminosity B factory.

- Monolithic Active Pixel Sensor (MAPS).
  The technology is potentially very suitable for low-energy high-luminosity colliders. The thickness of the detector is typically 300μm, but can be thinner, down to 100μm with routine etching technique at no cost, and down to 20μm with a special technique called anisotropic etching. The desired pixel size of 50 μm $\times$ 100 μm can be realized. Since MAPS has a build-in amplification capability, the readout electronics can be drastically simpler. The technology, however, is still not mature and active R&D is required.

We plan to make a thorough investigation of each technology to set the direction of the R&D. Figure 4.3 shows an example of a possible configurations for the vertex detector.

4.3 Tracking Detector

The most critical issue in choosing the tracking device for the experiment at Super KEKB is whether the normal gas wire chamber works as a central tracker, even in a higher beam background condition. A large wire chamber can be built with the established technology, which covers a large solid angle and provides good performance in both spatial and specific ionization loss (dE/dx) measurements. This section describes this issue, namely the aging effect and occupancy.

The accelerator design assumes beam currents of 10-times as large as that available at the present KEKB to achieve L =10^{35} cm^{-2}sec^{-1}, leading to a 10-times larger background rate.

The hit rate for the present Belle CDC at the highest beam current is shown in Fig.4.4, where the hit rate at the innermost layer exceeds 100 kHz. This layer works with a short enough dead time under this condition. The integrated charge on sense wires in the inner most layers for two years of operation exceeds 0.1 Coulomb/cm, which is close to the limit of radiation robustness of the gas wire chamber. No significant degradation of the gas gain has been observed. The dark current without the beams is still quite small. From these experiences, it is concluded that that the gas chamber works well even at a high

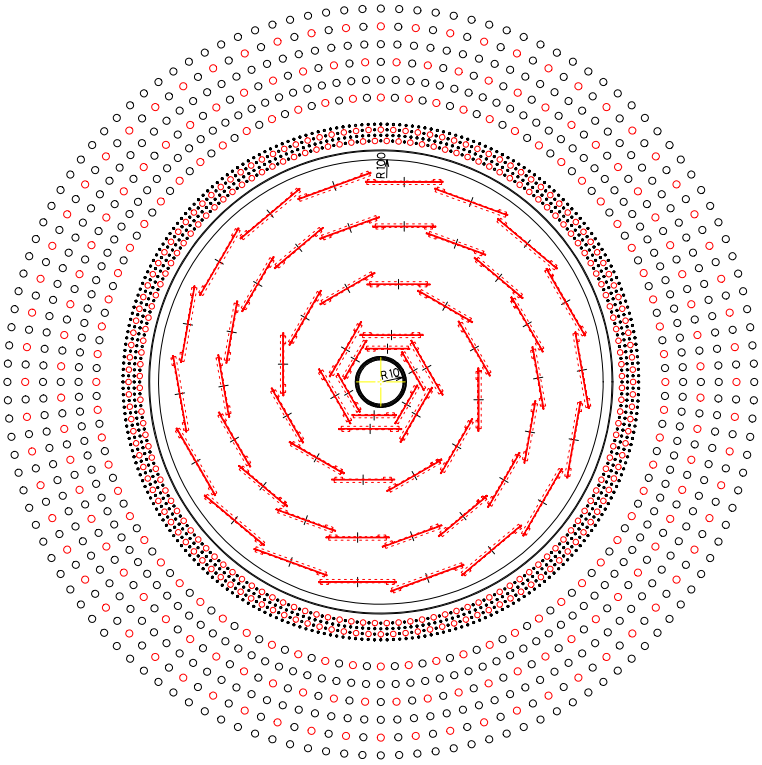

Figure 4.3: An rϕ view of the new pixel detector (inner two layers) surrounded by three layers of silicon strip detectors and a drift chamber.

rate around 100 kHz. As shown in Fig.4.4, the hit rates are around 5 kHz in most of the layers, which is extrapolated to 50 kHz in Super KEKB. This is below the hit rate of the innermost layer of the present CDC.

From these considerations, we conclude that the gas chamber survives and works as a tracking device at a radius larger than 150 mm.

Next, we estimate the occupancy of the wire chamber, which is relevant to the track reconstruction efficiency. The maximum drift time is approximately 400 nsec for the present CDC with a cell size of 18 mm. If we assume a chamber with the same cell size, the occupancy can be calculated by a simple extrapolation, 50 kHz$\times$400 nsec = 0.02. A 2% occupancy is manageable, but is marginal. In order to reduce the occupancy, there are two possible modifications. The first is to construct a drift chamber with smaller cells, which would make the hit rate lower and the maximum drift time shorter. R&D for a small cell chamber with a cell size of 5 mm is on-going.

The second is to use a gas with a faster drift velocity. In order to select a proper gas, we measured the drift velocities and pulse-height distributions with several types of gas mixtures for electron tracks. The results are shown in Figs. 4.5 and 4.6. One good candidate is pure methane, which has a radiation length similar to that of a 50%He-50%C_2H_6 mixture, which is used at present. Compared with the present gas mixture, the drift velocity with methane is faster by a factor of two, while the dE/dx resolution is almost the same.

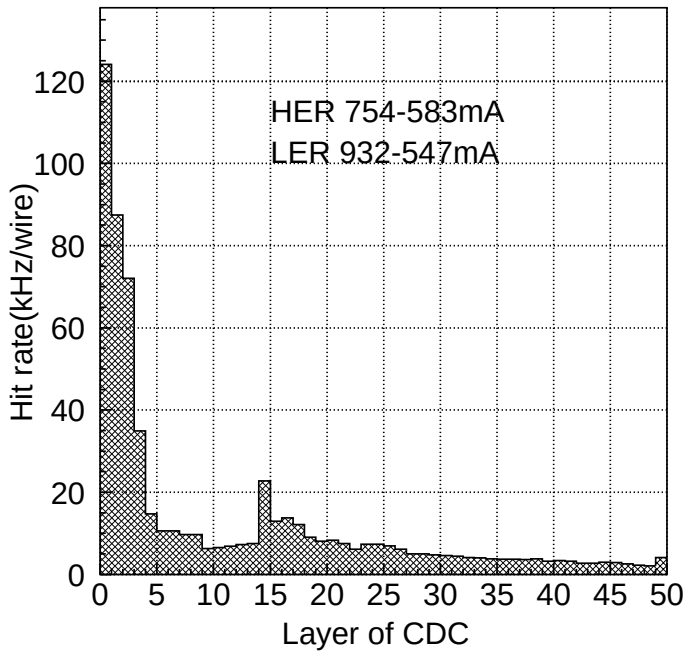

Figure 4.4: Hit rate as a function of the layer number for the present CDC at the maximum beam current.

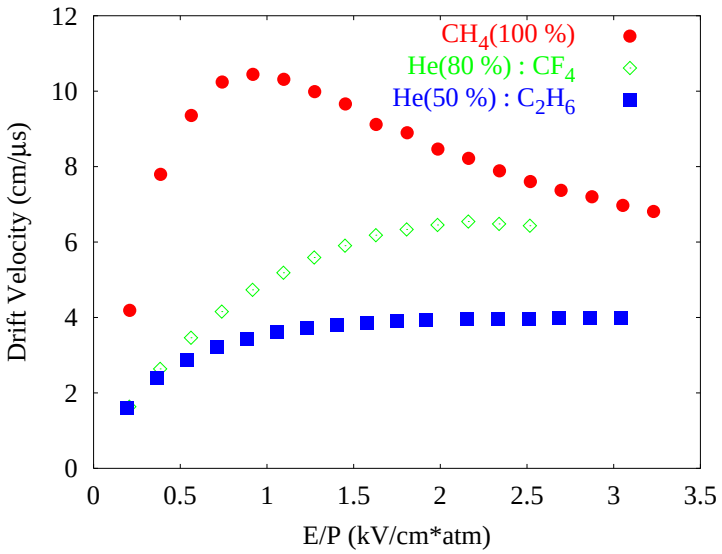

Figure 4.5: Measured drift velocity for candidate gas mixtures. The drift velocity for the present gas is shown as a reference.

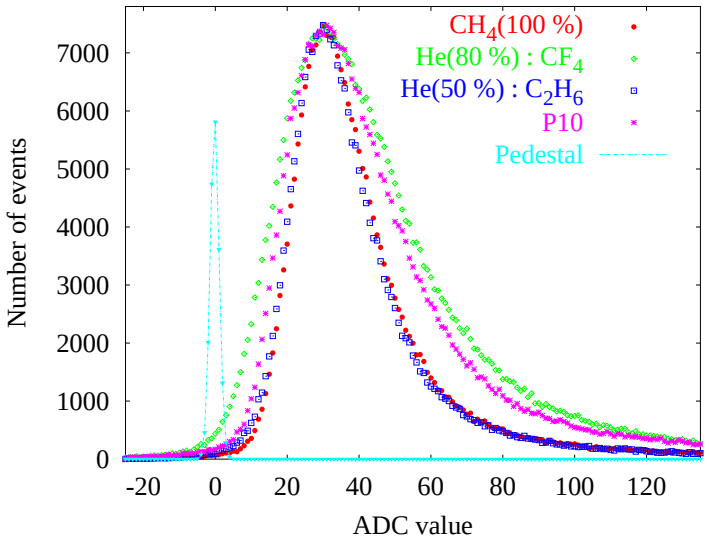

Figure 4.6: Measured pulse-height distribution for candidate gas mixtures. The data on the present gas and an Argon based gas are shown as a reference.

4.4 Particle Identification

Particle identification, in particular the K/π separation, plays a crucial role at B-factory experiments. This situation will also remain unchanged at the Super KEKB experiment. In order to meet these requirements, the detector system must be able to separate K/π mesons up to 4 GeV/c.

At present, K/π identification is carried out by combining information from three sub-detectors, dE/dx measured by the CDC, time-of-flight counters (TOF) and threshold aerogel Cherenkov counters (ACC). As for ACC, the refractive index of aerogel radiators varies from 1.010 to 1.028 in the barrel part to match the K/π momentum from the two-body decays, whereas it is 1.030 in the endcap part, making it useful only for flavor tagging. This detector system has provided about 88% kaon efficiency and about 8.5% pion fake rates.

There are two major concerns regarding the present Belle PID system, when it is used in a $10^{35}\mathrm{cm}^{-2}\mathrm{s}^{-1}$ high-luminosity environment: the radiation hardness of the detector materials and the detector dead time due to a high counting rate. By scaling the present dose at the CsI calorimeter ($\sim$ 20 Rad), the dose may reach an order of 10^3 to 10^4 Rad in 10 years of operation. The aerogel radiator was already tested up to 10 MRad irradiation, and no change in the refractive index and transparency was observed [93]. The transmission of the borosilicate glass window of a PMT was observed to drop to 20% at 400 nm wavelength with 10^5 Rad irradiation [94]. Also, the PMT gain may drift due to current stress. The TOF scintillator may suffer some damage at 10^4 Rad. These problems have to be investigated further.

At a higher counting rate, the detector dead time may be significant. Table 4.3 shows the dead time of the TOF, barrel and endcap ACC, which are estimated for 10-times higher counting rates than the present condition. Although it is hard to estimate the background rates, the TOF dead time will become significant.

For improving the particle-identification performance, it is desired that we replace

Table 4.3: Expected dead time of the TOF, barrel and endcap ACC at present and at a higher counting rate.

	TOF	BACC	EACC
Present rate	30kHz	1kHz	5kHz
Dead time (present)	0.3%	0.01%	0.05%
$\times$ 10	3.0%	0.1%	0.5%

the detectors by ring imaging Cherenkov detectors. For this purpose, two types of new detectors are considered: a *TOP Counter* (Time Of Propagation ring imaging Cherenkov counter) and a *Proximity Focusing Aerogel RICH*.

The TOP counter [95] utilizes the total internal reflection of Cherenkov photons produced in a quartz bar, as in the case of BaBar's DIRC detector. In contrast to the DIRC, which uses a large water stand-off box with phototubes for photon ring detection, the two-dimensional information of the ring image is represented by the TOP (time of propagation) and the horizontal emission angle (Φ) of the Cherenkov photons. Figure 4.7 shows the concept of the TOP counter. When a charged particle passes through the quartz radiator bar, Cherenkov photons are emitted in a conical direction defined by the emission angle (θ_c), transported to the end of the bar by means of total internal reflection, and then horizontally focused by a butterfly-shaped mirror onto a photodetection plane. Multi-anode PMT's are used to measure TOP as a function of the Φ angle. In this

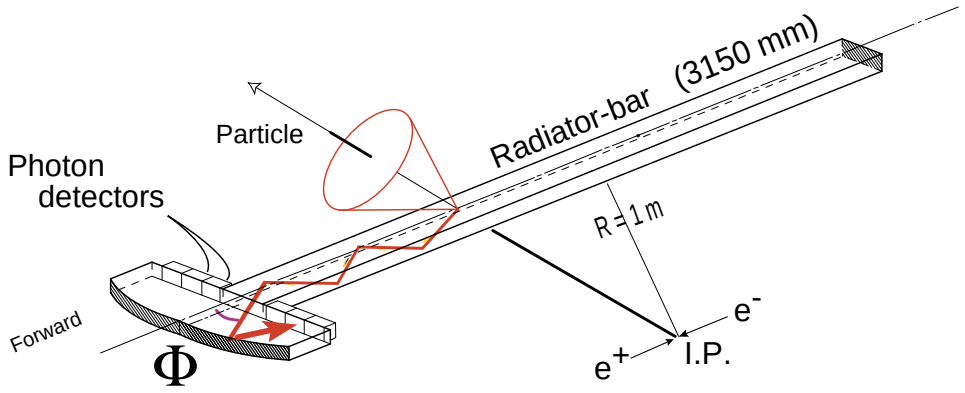

Figure 4.7: Concept of the TOP counter.

scheme, TOP is calculated as

$$TOP = \frac{L}{c/n} \cdot \frac{1}{sin\theta_c} \cdot \frac{1}{cos\Phi}\,, \tag{4.1}$$

where L is the distance from the emission point to the end of the bar. Therefore, the

Cherenkov emission angle (θ_c) can be deduced if both TOP and Φ are measured. In a sense, the TOP counter functions as a high precision TOF counter, where the finite duration of scintillation light emission is removed and also the arrival time is measured for every photon in an event. In order to have sufficient resolution to separate particle species, a transit time spread (TTS) of less than 100 ps is desired. Another concern is the flatness control of the quartz bar to preserve the initial emission angle of the Cherenkov radiation.

A simulation study shows that more than 3 σ K/π separation can be obtained up to 4 GeV/c with 75ps TTS for a single photon. Tests of a prototype counter are in progress using multi-anode PMT's (Hamamatsu R5900-L16). In a beam test, the obtained K/π separation was 3.6σ, even with only 20% of the photodetection plane covered by the PMT effective area.

The high optical quality of aerogels developed for the present Belle ACC has brought a new trend of ring-imaging Cherenkov counters, based on aerogel radiators and visible-light photodetection. A proximity focusing aerogel RICH detector is under consideration in order to improve the particle-identification performance in the endcap region, where the present Belle PID system does not have a useful K/π separation in the high-momentum region. Figure 4.8 shows the concept of the aerogel-RICH detector. The unique feature of the detector is the proximity focusing geometry, where the Cherenkov photons emitted from the radiator are directly detected by a photodetector array. The advantage of a detector with this geometry is its compactness, which is especially important for experiments at colliders. The aerogel radiator must be relatively thin (~ 2 cm) so that the deterioration of the Cherenkov-angle resolution due to the ambiguity of the photon emission point is minimized. The key issue is the light yield, since the Cherenkov radiator must be thin,

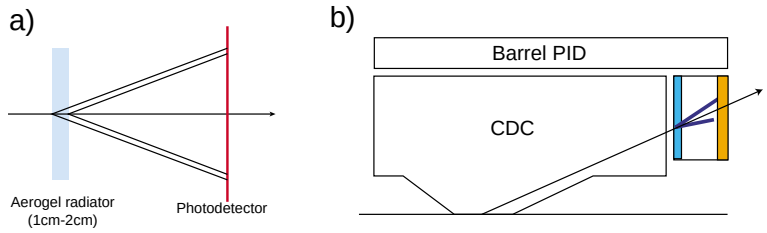

Figure 4.8: Concept of the proximity focusing aerogel RICH detector.

as noted above. The photodetector must have a sufficient single-photon sensitivity in a strong magnetic field, and also must cover a large area. The short wavelength component is highly suppressed due to Rayleigh scattering inside the aerogel radiator; therefore, position-sensitive photodetectors in the visible light region, such as a multi-anode PMT, equipped with fine-mesh dynodes, and a hybrid photodiode (HPD) pixel would be an appropriate choice.

The simulation indicates that $N_{pe} > 12$ is possible for particles with $\beta \approx 1$. A lower index ($n = 1.030$) gives a better separation, but the light yield for pions at around 0.8 GeV/c may be critical. A K/π separation of more than 5σ at 4 GeV/c is possible.

In order to prove the principle of the proximity focusing aerogel RICH and also to test the above simulation results, the test counter shown in Fig. 4.9-a) has been built. For photodetection, an array of multi-anode PMT's (Hamamatsu R5900-M16) is used.

Cosmic ray and beam tests are in progress to test the light yield and Cherenkov-angle resolution. Figure 4.9-b) shows the ring image produced by cosmic rays.

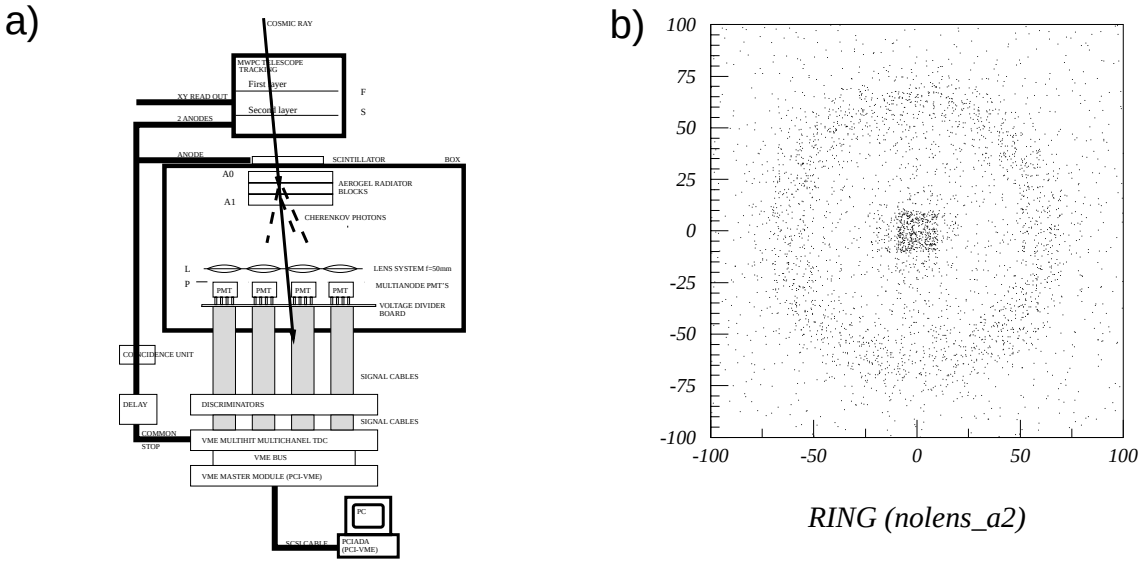

Figure 4.9: a) Setup of a cosmic-ray test bench for the aerogel RICH detector. b) Observed Cherenkov ring image.

4.5 Electromagnetic Calorimeter

The present EM calorimeter [90] of Belle is composed of a 3.0m long, 1.25m inner-radius barrel part and annular endcaps placed along the beam line at +2.0m and −1.0m from the beam-beam interaction point (IP). Each CsI(Tℓ) counter has a tower-structure shape of which the cross section is about 6 cm×6 cm and the length is 30 cm. The entire system contains 8,736 counters and weighs ∼43 tons. The readout of each counter is made via an independent pair of silicon PIN photo-diodes (PD's) and charge-sensitive preamplifiers attached at the rear surface of the crystal.

In Super KEKB, we expect larger beam backgrounds to the EM calorimeter, which would degrade its performance. The effects of the beam backgrounds on the EM calorimeter are classified into the following three categories: (a) incoherent pileup noise in each of the crystal blocks due to the soft background, (b) fake energy clusters due to hard γ's, and (c) radiation damage of the crystal. Here, (a) is roughly proportional to the beam current, while (b) and (c) are proportional to its square.

A crystal detector with faster light output is favorable from the point of view of reducing any background effects. Using pure CsI crystal for the endcap calorimeter is one of the attractive options in this sense. However, in this report, we assume to use the existing calorimeter in the endcap, and design the upgraded calorimeter with the following constraints.

- CsI(Tℓ) crystal with PD's and preamps.

	(a) Expected σ_{noise} from current scheme	(b) Expected σ_{noise} from optimized filtering	(b)/(a)
barrel	2.5MeV	1.25MeV	50%
forward endcap	5MeV	2 MeV	40%
backward endcap	8MeV	3MeV	38%

Table 4.4: Expected noise ($\sigma_{\rm noise}$) using the current scheme and optimized filtering.

	noise per crystal in r.m.s. (σ_{noise})	E_γ= 50MeV	E_γ= 100MeV	E_γ= 1,000MeV
barrel (now)			5%	$\sim$ 2%
barrel part	1.2−2.5MeV	9−13%	5−9%	$\sim$3%
inner backward endcap	3−8MeV	15−33%	10−20%	3−5%
at 10^{35}cm^{-2}s^{-1}				

Table 4.5: Expectation of the γ energy resolution (σ_E/E) at 10^{35}cm^{-2}s^{-1}.

- Pipeline readout, which would allow flexible data taking without any dead time.
- Wave-form recording, which is expected to provide better energy resolution.

In this new scheme, the pileup noise is expected to be reduced, as shown in Table 4.5 for $L = 10^{35}$cm^{-2}sec^{-1}. These estimates are based on measurements of the noise ($\sigma_{\rm noise}$) in the present calorimeter: 300 keV (barrel part), 600 keV (forward endcap) and 1 MeV (backward endcap) at $L = 1.5 \times 10^{33}$cm^{-2}sec^{-1}.

Table 4.5 summarizes the expected the degradation of the γ energy resolution. Since the γ energy resolution (5−9%) at 10^{35}cm^{-2}sec^{-1} is not worse than twice the current resolution (5%) for E_γ=100 MeV, as shown in Table 4.5, degradation in barrel region is acceptable.

The current rate of fake γ's from the beam background is measured by using randomly triggered events. Fig. 4.10 shows the energy distribution of γ's in those events in the polar angle region $17^\circ < \theta < 150^\circ$ when the luminosity is 3.5×10^{33}cm^{-2}sec^{-1} and the $e^+(e^-)$ beam current is 750 mA (650 mA). The number of γ's in the barrel region is about 40% of the total region. The average γ energy is 35 MeV.

Fig. 4.11 shows the average values of the summed γ energies per event ($E_{\rm sum}$) as a function of the γ energy threshold. This measurement is extrapolated to $L = 10^{35}$cm^{-2}sec^{-1}, as summarized in Tables 4.6 and 4.7.

The radiation dose has been determined by integrating the instantaneous increase of the PD bias current. We observed 5 Rad for the barrel part, and 20 Rad for the inner endcaps. For about 30fb^{-1} integrated luminosity, losses of light output by 1.5% and 3% have been observed for the barrel part and the innermost endcap parts, respectively. This result is consistent with that obtained at the R&D stage, as shown in Fig. 4.12 [99].

For 3,000fb^{-1}, which is a 100-times larger integrated luminosity than at present, only 5$\sim$10% light output degradation is expected, for which the radiation dose is expected to

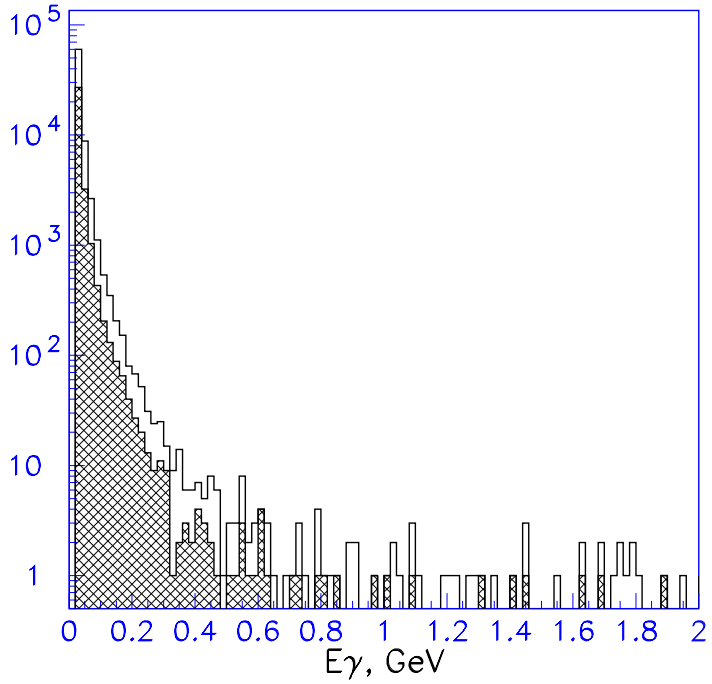

Figure 4.10: Energy distributions for γ's from randomly triggered events recorded with Belle. The open histogram is for γ's between 17° and 150° in θ (all part) and the shaded one for γ's between 32° and 130° (barrel part).

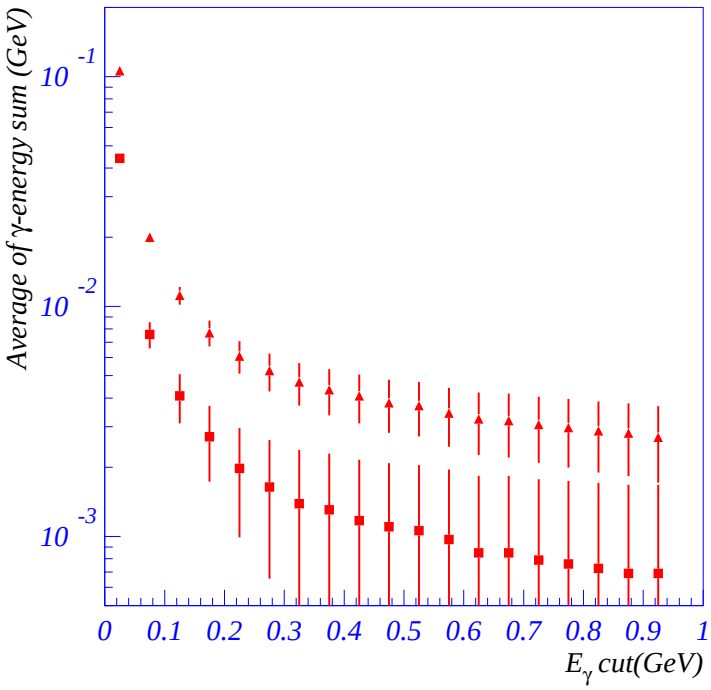

Figure 4.11: Average of the summed γ energies (GeV) per event ($E_{\rm sum}$) as a function of the γ energy threshold (GeV) from randomly triggered events recorded with Belle. The solid points are for γ's between 17° and 150° in θ (all part) and the dashed ones for γs between 32° and 130° (barrel part).

cut	N_γ(now)	Expected N_γ(current scheme) at $10^{35}\mathrm{cm}^{-2}\mathrm{s}^{-1}$	Expected N_γ(optimized filtering) at $10^{35}\mathrm{cm}^{-2}\mathrm{s}^{-1}$
E_γ >20MeV(all)	3.0	60∼1,200	15∼300
(barrel)	1.3	26∼520	6.5∼130
E_γ >72MeV(all)	0.14	2.9∼58	0.7∼14
(barrel)	0.056	1.1∼22	0.3∼5.6
E_γ >123MeV(all)	0.044	0.9∼18	0.2∼4.4
(barrel)	0.018	0.4∼7.2	0.1∼1.8

Table 4.6: Numbers of γ's per event (N_γ) with various E_γ cuts for all parts and the barrel part. The present numbers, the expected numbers with the current scheme and those with optimized filtering at $10^{35}\mathrm{cm}^{-2}\mathrm{s}^{-1}$ are shown.

cut	E_{sum}[GeV](now)	Expected E_{sum}[GeV] at $10^{35}\mathrm{cm}^{-2}\mathrm{sec}^{-1}$ (current scheme)	Expected E_{sum}[GeV] at $10^{35}\mathrm{cm}^{-2}\mathrm{sec}^{-1}$ (optimized filtering)
E_γ >20MeV(all)	0.1	2.∼42.	0.5∼11.
(barrel)	0.04	0.9∼18.	0.2∼4.
E_γ >72MeV(all)	0.02	0.4∼8.	0.1∼2.
(barrel)	0.008	0.15∼3.	0.04∼0.8
E_γ >123MeV(all)	0.01	0.2∼4.5	0.3∼1.1
(barrel)	0.004	0.08∼1.6	0.02∼0.4

Table 4.7: Average of the summed γ energies per event (E_{sum}) with various E_γ cuts for all parts and the barrel part. The present numbers, the expected numbers with current scheme and those with optimized filtering at $10^{35}\mathrm{cm}^{-2}\mathrm{sec}^{-1}$ are shown.

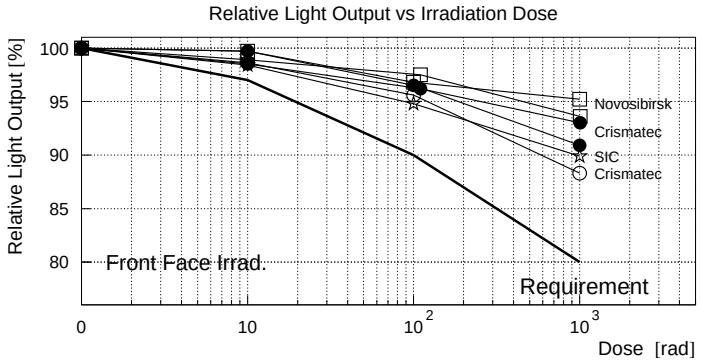

Figure 4.12: Radiation damage to CsI(Tℓ) counters. Light output change as a function of the dose for front face irradiation. The light output values are normalized to those before irradiation. The thick line represents the requirement for the radiation hardness of the Belle EM calorimeter.

be about 1 kRad. We expect no significant degradation in performance with the gain calibration of the light output presently applied,

4.6 Data Acquisition System

The data acquisition system of Belle [100][101] consists of the three components: front-end readout systems, an event-building and online trigger complex, and a mass storage system. It records 40 kB events at a rate of 300 Hz. This global structure could be applied to the DAQ system of an experiment at Super KEKB. The physics event rate scales with the luminosity, while the background rate, which is usually very difficult to estimate, is assumed to be proportional to the sum of the beam currents. As for the event size, we expect some increase for two reasons. One is due to the introduction of a more finely segmented detector such as a pixel silicon detector. The other is due to an increase in the occupancy. Considering these points leads to the expected trigger rate of 3 kHz, and the required design trigger rate of 6 kHz, including a factor of two margin for the background. The data size is assumed to be 2.5-times larger, or 100 kB for both physics and background events. Before recording data, there will be online event filtering, which should remove three quarters of the background events. These parameters are summarized in Table 4.8.

Table 4.8: Design specification of the current and new data acquisition systems.

	$5 \times 10^{33}\mathrm{cm}^{-2}\mathrm{s}^{-1}$		$1 \times 10^{35}\mathrm{cm}^{-2}\mathrm{s}^{-1}$	
	typical	design	expected	design
Background rate	200 Hz	500 Hz	2 kHz	5 kHz
Physics rate	50 Hz	100 Hz	1 kHz	1 kHz
Data size	40 kB	30 kB	100 kB	100 kB
Data flow at L1	10 MB/s	40 MB/s	300 MB/s	600 MB/s
at storage	5 MB/s	24 MB/s	150 MB/s	225 MB/s

Although the existing system shows satisfying performance under the current running condition, there are several conceptual problems that have to be solved to be used in the Super KEKB.

The first and the most severe limit would be in the front-end electronics and their readout. In the current FASTBUS-TDC based system, the TDC data are read out in series, taking 100 μs in total to read out one event. This is far too long when we need to handle trigger rate 10-times larger, and it cannot be absorbed by a simple trick, like further parallelizing the system by a factor of a few. Therefore, it is unavoidable to give up the current readout scheme and to develop a new deadtime-less readout scheme with pipelined buffers, as used in hadron collider experiments.

The second limit concerns data storage. In order to keep the analysis as simple as possible, it is preferable to record one run on a single tape. However, considering the storage rate of 200 MB/s, it is not likely that there will be a mass storage device that can handle such a recording rate. Assuming that the tape drive can only write 40 MB/s, which is the expected performance of the next generation of the current device, we must use at least 5 drives in parallel.

The last limit is in the event-building farm. The event-building farm system based on a fast network and PC's, which was recently introduced in Belle, is not scalable to the 10-times larger data rate with the present configuration, even if we assume a factor of 3 to 4 improvement in the PC performance. Here, however, we can rather easily consider several different configurations to parallelize the data stream to cope with the data rate.

The basic idea of the pipelined readout is to introduce two levels of pipelines, as shown in Fig. 4.6. The first pipeline is to gain time for the trigger decision, either by a digital

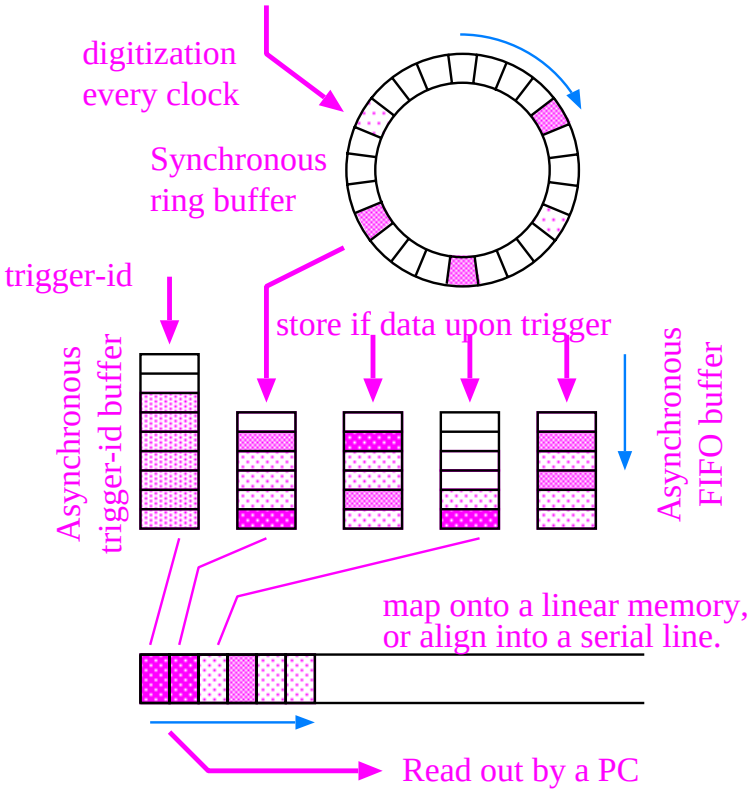

Figure 4.13: Pipeline system for the deadtime-less readout system.

buffer after a flash-ADC readout or by an analog buffer to keep the signal pulse height. The second pipeline is to keep the triggered data until it is read out. The first pipeline forms a ring-buffer with a free-running system clock. The size of the pipeline is determined by the time for the trigger decision divided by the clock cycle. The minimum clock cycle is determined by the time to store the signal into the pipeline buffer, while a longer clock cycle might be preferred to reduce the size of the pipeline buffer.

The second pipeline is to convert the synchronous digitization in timing to an asynchronous handling of the readout sequence. The digitization must take place for all of the readout channels, but the readout should be made only for those channels that contain signals. From a readout point-of-view, those sparsified data should be mapped into a continuous memory buffer or transmitted over a serial line. The depth of the pipeline is determined by the expected maximum readout latency times some margin factor. For each trigger decision, at least the trigger-id has to be stored in a trigger pipeline. The signal for each channel is stored in an independent pipeline with a trigger-id tag, and therefore the pipeline depth can be the depth of the trigger-id pipeline times the expected maximum occupancy times some margin factor.

The readout takes place either through conventional VME readout or a recently developed serial-bus (USB 2.0 or IEEE1394). In each case, the readout modules should be packed into some backplane-type system, like VME, for initialization, control and monitoring that are independent of the data readout path. One unit of such a system should handle at least one thousand channels, and be read out by a single PC (or embedded CPU board). For the case of the serial bus-type readout, more readout paths will be required to satisfy the required bandwidth, which is expected to be 30 MB/s/unit.

The current event-building farm system consists of 7 PC's (Fig. 4.6-left); also, we assume that 5-times more PC's are needed to handle the 10-times larger data bandwidth. The current system is not really scalable by a factor of 5, or to make a 15 layer-1 nodes inter-connected to 15 layer-2 nodes, primarily due to the limitation from the number of network ports pluggable in a single PC.

One possible work-around is to consider the current 7 PC's as a "unit" and to distribute the data into 5 of such units (Fig. 4.6-right). Then, one PC of layer-1 has to receive data from 10 readout PC's with 1/5 bandwidth each.

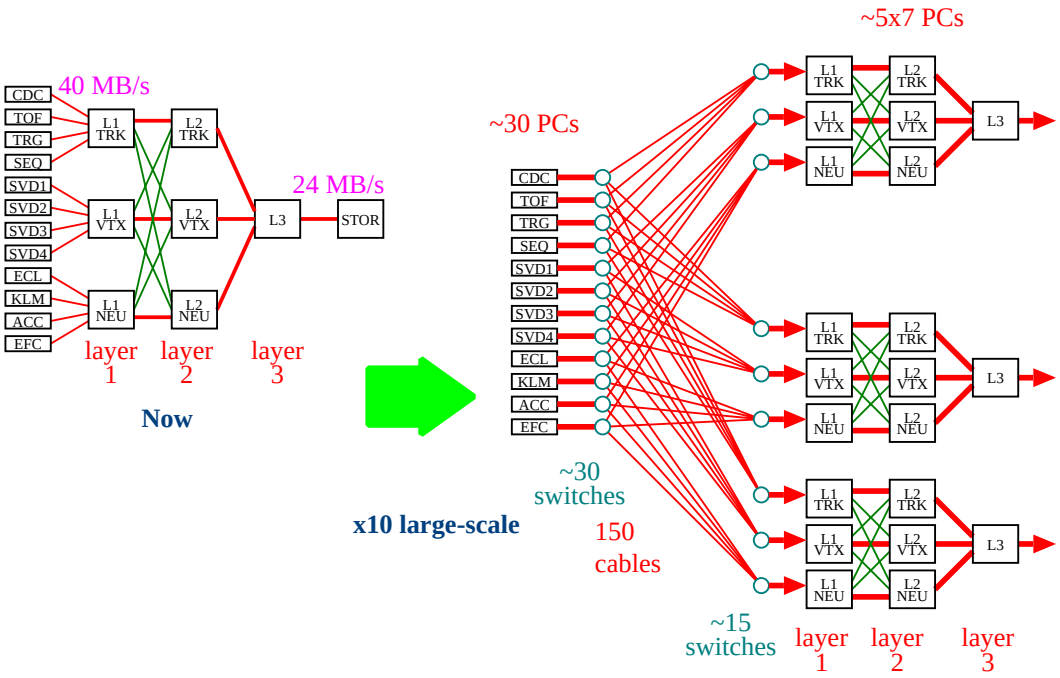

Figure 4.14: Large-scale event-building farm using the current system as a "unit."

Since it is desirable to split the event-building data flow into several paths, it is also necessary to split the data recording flow into multiple paths, as we anticipate that no single drive can handle the required data recording speed. What is needed here is a disk buffer that can keep the entire data of a run for a single event-building farm unit, and later-on stream merging from multiple disk buffers to a single tape. In order to achieve a data acquisition speed of 200 MB/s, for example, 5 tapes of 40 MB/s have to be recording in parallel. Therefore, while one disk is being written at full speed, 5 disks are read out in parallel with 1/5 speed. More than 6 drives are needed, including some allowance for runs of different sizes; disk caching with 10 disks for 5 drives could provide a reasonable margin and less complexity, because the disk-to-tape connection can be fixed at 2-to-1 (Fig. 4.6).

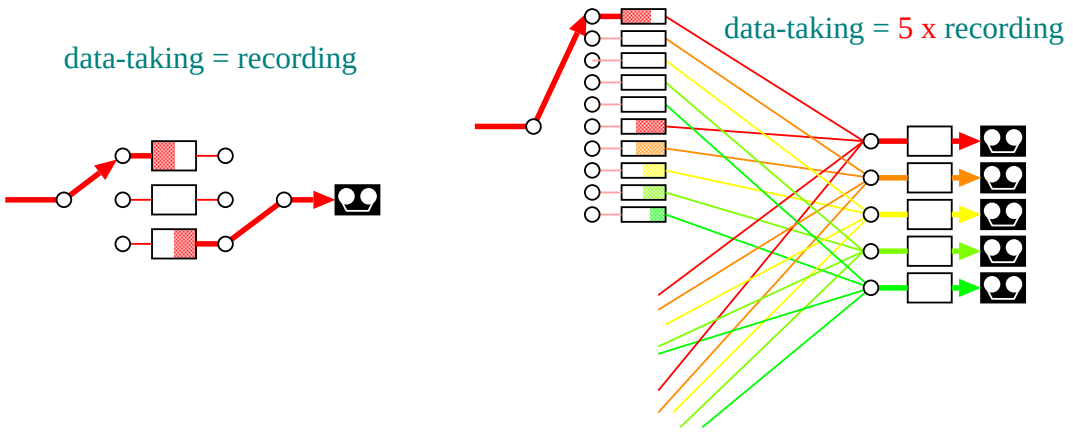

Figure 4.15: Storage caching with an equal speed tape drive and 5-times slower tape drives.

The required size of the disk is 200 GB/run, which is just two-times larger than the currently available largest single drive. As many as 50 disks, totaling 10 TB, are required.

The network solution will require 5 units of 1-to-10 Gigabit Ethernet switch (12 port or more), just for switching. Since only one connection will be used at a time, an inexpensive switch is sufficient for this purpose.

Finally, it is already more or less feasible to construct the latter half of the system, if we give up the expected factor of two to three improvement in the performance of each device. The replacement of the current electronics with the new pipeline based front-end readout system, however, requires completely new electronics development, and is not trivial at the moment. In order to start installation in the year 2006, we need to have a prototype design within a year or two from now.

4.7 Computing Requirement

At a luminosity of $10^{35}\mathrm{cm}^{-2}\mathrm{s}^{-1}$, the production rate of $B\bar{B}$ is 100 Hz. By adding other physics trigger rates, we expect to write events at an average rate of 1 kHz. The average event size may go up to 100 kB. Thus, the average data rate will be 100 MB/s. We assume that the maximum trigger rate is 6 kHz, the maximum data rate is 600 MB/s and the live time is 2×10^7 second per year. Under these assumptions we will accumulate up to 2 PB per year. We are confident that the online/off-line data reduction can be as efficient and effective as now, and can further reduce the size of data that must be permanently stored to less than half. The requirement for the storage of raw and "data summary on tape"(DST) data, therefore, is 2 PB per year. The data-storage system should be at least as large as 10 PB at the beginning, and be expandable if necessary.

The average input data rate of 100 MB/s is modest. The future generation of the current tape drive used for the Belle data-acquisition system, the SONY DTF–2 tape drive, is expected to quadruple the current writing speed of 24 MB/s up to 100 MB/s. However, the maximum rate of 600 MB/s requires parallel streams. We therefore plan to have an online event buffer.

For calibration and data monitoring, we would like to keep the raw data available online for one week or so. This would serve as a buffer for the tape storage system as

well. At the maximum data rate of 500 MB/s for 5×10^5 seconds per week, the size of the buffer should be at least as large as 250 TB. A buffering system of this size with a maximum of 1 GB/s transfer rate will not be difficult in 4–5 years using commodity PC's and hard disks available at that time.

Belle currently has a 300 GHz equivalent Pentium PC farm at KEK. This system can produce DSTs at a maximum rate of a little less than 1 fb^{-1} per day, and, on average, 20 fb^{-1} per month. The current rate at which the KEKB accelerator system produces data is 0.24 fb^{-1} per day at the maximum rate of 6 fb^{-1} per month. A thirty-fold increase in the luminosity is expected for the Super KEKB. With this luminosity increase it, in principle, only requires a 3,000 GHz Pentium PC farm to catch up with the DST production at the current level of complexity. However, experience tells us that for a factor of 10 to 20, even 50-times more CPU time is often necessary. Consider the situation that at the time we accumulated 3 ab^{-1} we made a breakthrough in reconstruction software and suddenly we must reprocess the entire DST data. At the same time we must generate full GEANT Monte Carlo (MC) events with a 3-times larger sample size, say, 10 ab^{-1}. If we only have twice the CPU power to catch up with the daily production by the KEKB accelerator, it would take 12 years to reprocess the entire data sample and to generate the necessary MC events in parallel with the daily production. To finish the reproduction and MC generation in three months, we need 50-times more CPU power than the current one to catch up with the daily production. We therefore estimate that, to be competitive, we need several tens of thousands of GHz equivalent Pentiums for the PC farm. The requirements for the computing system are:

1. We must be able to reprocess all of the data taken in the previous 3–4 years within three months.

2. Some of the physics analysis processes should be moved upstream into the data-processing production job as they become standard.

3. Production and physics analysis jobs will become more complex, heavy on CPU, and be repeated more frequently as we come to understand the detector and move to precision measurements and B-decay-to-many-body physics processes.

4. The assumptions from industry are as follows. The CPU clock speed will become twice as fast in 18 months. However, the normal maintenance contract of the PC's cannot be extended for more than 3 years. At the time of purchase, the fastest processor is quite expensive and not always the best in terms of cost per performance.

5. The technology used to store data may change from tape to something else, for example disks.

6. The new infrastructure, i.e., building, wall power and cooling systems, and the network and security system will have to be considered.

Experience tells us that the complexity, and thus the CPU requirement for each event, increases at a rate of about 20% every year. Fig. 4.16 shows the integrated luminosity multiplied by the complexity factor and the expected clock speed of the CPU.

Currently, the size of the compressed hadron data for 1 fb^{-1} is 150 GB. A single copy of such data would require 150 TB/year of running. We probably need 1−2 PB of online disks. If we chose to attach commodity hard disks to each node of the PC farms,

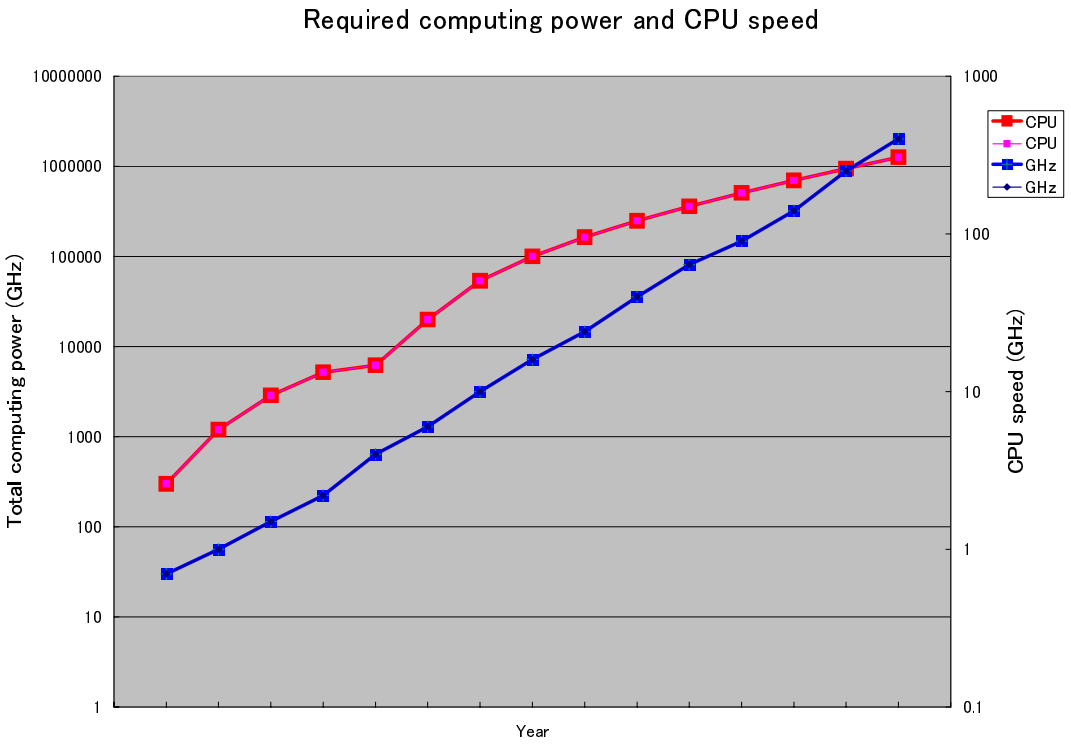

Figure 4.16: Required computing power for the DST production and MC generation and the estimated CPU clock speed for the next 15 years

500 GB to 1 TB per PC would be sufficient. This is modest, considering that the size of a commodity hard disk could hold as much as 400 GB to 1 TB of data in five years. With several to tens of thousands of PC's, we could distribute data on the PC's, and therefore avoid large and expensive disk systems. However, we must develop software to deal with the distribution of the data over the local disks of tens of thousands of PC's.

By a mass storage system we mean a system to keep data from Belle permanently. The size of the mass storage system will be at least 10 PB at the beginning and would be expandable. As discussed in the previous section, the tape drive will quadruple the capacity and speed. If we can use 800 GB tapes, the size of the storage system is only five-times larger than the current system which holds 2500 tapes (500 TB) in a tape library. Considering the current cost of the tape system, it could cost as much as 30 million dollars.

On the other hand, 10 PB of data can be held on 10,000 1 TB disks that are attached to the PC's. In this way, we may be able to do without a large, expensive tape library system. However, all of the hard disks will fail in a few to several years, and managing the data on such devices with such a high failure rate could be a nightmare. Unless we have a very reliable software system that can manage the integrity of the experimental data, we feel that it is unsafe to keep all of the data only on hard disks. There might be an intermediate solution, and we will certainly consider it to reduce the overall cost of the computing system.

Connecting the proposed PC farm with the mass storage system and the DAQ system requires a fast, reliable network system. Although 10 GbE UTP copper cable is the most

desired situation, we will have to see what happens. The input from the DAQ system requires 500 MB/s, and the input/output to and from the mass storage system also requires a 5−10 GB/s aggregate. We consider these modest requirements. The transfer speed between the nodes in the PC farm does not require more than GbE speed of several tens of MB/s. However, connecting among several tens of thousands of PC nodes will require a large, and therefore, expensive network switch.

The foot print of the above system is five to 10-times larger than what we already have in the computing research center. We would need a new building of a few to several thousand square meters to hold such a computing system.

The data-management software will be very complex, even if we keep the serial IO model, which has been used at Belle. The GRID computing architecture has become popular in recent years and may be applicable to Belle. We have started to investigate this possibility.

The computing system used in the experiment at Super KEKB will have to be large and complex, because the amount of data and the complexity of the physics analysis will be on an order of magnitude or two more than those of the current generation of experiments. Even with the expected advances in computing industries, the cost to manage the complex physics data analysis with the huge amount of data will be high. Of course, although careful planning is the key, the development of software to manage such a system will require man power. It certainly is a very challenging job to build such a computing system.

Chapter 5

Conclusion

The physics opportunities at a B factory operating at the luminosity of $10^{35}\mathrm{cm}^{-2}\mathrm{s}^{-1}$ are very attractive. The precise determination of the CKM matrix elements as well as a search for New Physics can be explored in studies of the B meson system. Super KEKB will complement the direct search at high energy colliders. Studies of properties of rare B meson decays to modes that involve neutral particles can only be performed at e^+e^- machines.

The unprecedented luminosity of $10^{35}\mathrm{cm}^{-2}\mathrm{s}^{-1}$ appears to be feasible with a major upgrade of the existing KEKB facility. The machine can be upgraded on a time scale that makes its physics capability relevant with regards to the hadron collider experiments. The design calls for substantial amounts of research and development and pushes accelerator technology to its limit; thus it is a challenging and necessary step toward a new high energy e^+e^- machine.

The existing Belle detector can be upgraded in order to take a full advantage of the high luminosity of the KEKB machine. Improvements in the vertex resolution, tracking and photon finding efficiencies are essential to reduce backgrounds for the very rare decays with missing neutral particles.

When considering the next project in the field of high energy particle physics in Japan using an accelerator, an upgrade of KEKB and Belle for a precise test of the KM mechanism and search for New Physics beyond the Standard Model in the B meson system is one of the most attractive choices. The physics motivation is very compelling and the upgrade can be achieved at a moderate cost and on a reasonable time scale.

As a consequence of these considerations, we express our interest in upgrading the KEKB collider to Super KEKB in the year 2006, accompanied by an upgrade of the Belle detector.

Bibliography

[1] M. Kobayashi and T. Maskawa, Prog. Theor. Phys. **49**, 652 (1973).

[2] A. B. Carter and A. I. Sanda, Phys. Rev. Lett. **45**, 952 (1980).

[3] A. B. Carter and A. I. Sanda, Phys. Rev. D **23**, 1567 (1981).

[4] I. I. Bigi and A. I. Sanda, Nucl. Phys. B **193**, 85 (1981).

[5] B. Aubert *et al.* (BABAR Collaboration), Phys. Rev. Lett. **87**, 091801 (2001), [arXiv:hep-ex/0107013].

[6] K. Abe *et al.* (Belle Collaboration), Phys. Rev. Lett. **87**, 091802 (2001), [arXiv:hep-ex/0107061].

[7] K. Abe *et al.* (BELLE Collaboration), [arXiv:hep-ex/0109026].

[8] BELLE Collaboration, submitted to Phys. Rev. Lett.

[9] M. Ciuchini *et al.*, J.H.E.P. **0107** (2001) 13, [arXiv:hep-ph/0012308].

[10] Y. Grossman and M. P. Worah, Phys. Lett. B **395**, 241 (1997), [arXiv:hep-ph/9612269].

[11] R. Barbieri and A. Strumia, Nucl. Phys. B **508**, 3 (1997), [arXiv:hep-ph/9704402].

[12] T. Moroi, Phys. Lett. B **493**, 366 (2000), [arXiv:hep-ph/0007328].

[13] M. Gronau and D. London, Phys. Rev. Lett. **65**, 3381 (1990).

[14] A. E. Snyder and H. R. Quinn, Phys. Rev. D **48**, 2139 (1993).

[15] M. Gronau and D. London., Phys. Lett. B **253**, 483 (1991).

[16] M. Gronau and D. Wyler, Phys. Lett. B **265**, 172 (1991).

[17] D. Atwood, I. Dunietz and A. Soni, Phys. Rev. Lett. **78**, 3257 (1997), [arXiv:hep-ph/9612433].

[18] D. Atwood, I. Dunietz and A. Soni, Phys. Rev. D **63**, 036005 (2001), [arXiv:hep-ph/0008090].

[19] I. Dunietz, Phys. Lett. B **427**, 179 (1998), [arXiv:hep-ph/9712401].

[20] D. A. Suprun, C. W. Chiang and J. L. Rosner, [arXiv:hep-ph/0110159].

[21] D. London, N. Sinha and R. Sinha, Phys. Rev. Lett. **85**, 1807 (2000), [arXiv:hep-ph/0005248].

[22] M. Neubert and J. L. Rosner, Phys. Rev. Lett. **81**, 5076 (1998), [arXiv:hep-ph/9809311].

[23] Y. Y. Keum, H. n. Li and A. I. Sanda, Phys. Lett. B **504**, 6 (2001), [arXiv:hep-ph/0004004].

[24] Y. Y. Keum, H. N. Li and A. I. Sanda, Phys. Rev. D **63**, 054008 (2001), [arXiv:hep-ph/0004173].

[25] M. Beneke, G. Buchalla, M. Neubert and C. T. Sachrajda, Nucl. Phys. B **606**, 245 (2001), [arXiv:hep-ph/0104110].

[26] K. C. Bowler *et al.* (UKQCD Collaboration), Phys. Lett. B **486**, 111 (2000), [arXiv:hep-lat/9911011].

[27] A. Abada, D. Becirevic, P. Boucaud, J. P. Leroy, V. Lubicz and F. Mescia, [arXiv:hep-lat/0011065].

[28] A. X. El-Khadra, A. S. Kronfeld, P. B. Mackenzie, S. M. Ryan and J. N. Simone, Phys. Rev. D **64**, 014502 (2001), [arXiv:hep-ph/0101023].

[29] S. Aoki *et al.* (JLQCD Collaboration), [arXiv:hep-lat/0106024].

[30] A. F. Falk, Z. Ligeti and M. B. Wise, Phys. Lett. B **406**, 225 (1997), [arXiv:hep-ph/9705235].

[31] R. D. Dikeman and N. G. Uraltsev, Nucl. Phys. B **509**, 378 (1998), [arXiv:hep-ph/9703437].

[32] C. W. Bauer, Z. Ligeti and M. Luke, Phys. Lett. B **479**, 395 (2000), [arXiv:hep-ph/0002161].

[33] C. W. Bauer, Z. Ligeti and M. Luke, [arXiv:hep-ph/0107074].

[34] S. Bertolini, F. Borzumati, A. Masiero and G. Ridolfi, Nucl. Phys. B **353**, 591 (1991).

[35] A. Ali, G. F. Giudice and T. Mannel, Z. Phys. C **67**, 417 (1995), [arXiv:hep-ph/9408213].

[36] P. L. Cho, M. Misiak and D. Wyler, Phys. Rev. D **54**, 3329 (1996), [arXiv:hep-ph/9601360].

[37] T. Goto, Y. Okada, Y. Shimizu and M. Tanaka, Phys. Rev. D **55**, 4273 (1997), [arXiv:hep-ph/9609512].

[38] J. L. Hewett and J. D. Wells, Phys. Rev. D **55**, 5549 (1997), [arXiv:hep-ph/9610323].

[39] A. Ali, P. Ball, L. T. Handoko and G. Hiller, Phys. Rev. D **61**, 074024 (2000), [arXiv:hep-ph/9910221].

[40] C. S. Kim, Y. G. Kim, C. D. Lu and T. Morozumi, Phys. Rev. D **62**, 034013 (2000), [arXiv:hep-ph/0001151].

[41] S. Fukae, C. S. Kim and T. Yoshikawa, Phys. Rev. D **61**, 074015 (2000), [arXiv:hep-ph/9908229].

[42] C. S. Kim, Y. G. Kim and T. Morozumi, Phys. Rev. D **60**, 094007 (1999), [arXiv:hep-ph/9905528].

[43] A. L. Kagan and M. Neubert, Phys. Rev. D **58**, 094012 (1998), [arXiv:hep-ph/9803368].

[44] M. Aoki, G. C. Cho and N. Oshimo, Phys. Rev. D **60**, 035004 (1999), [arXiv:hep-ph/9811251].

[45] M. Aoki, G. C. Cho and N. Oshimo, Nucl. Phys. B **554**, 50 (1999), [arXiv:hep-ph/9903385].

[46] T. Goto, Y. Y. Keum, T. Nihei, Y. Okada and Y. Shimizu, Phys. Lett. B **460**, 333 (1999), [arXiv:hep-ph/9812369].

[47] D. Atwood, M. Gronau and A. Soni, Phys. Rev. Lett. **79**, 185 (1997), [arXiv:hep-ph/9704272].

[48] C. K. Chua, X. G. He and W. S. Hou, Phys. Rev. D **60**, 014003 (1999), [arXiv:hep-ph/9808431].

[49] S. Baek, T. Goto, Y. Okada and K. i. Okumura, Phys. Rev. D **63**, 051701 (2001), [arXiv:hep-ph/0002141].

[50] S. Baek, T. Goto, Y. Okada and K. i. Okumura, Phys. Rev. D **64**, 095001 (2001), [arXiv:hep-ph/0104146].

[51] J. M. Soares, Nucl. Phys. B **367**, 575 (1991).

[52] C. Greub, H. Simma and D. Wyler, Nucl. Phys. B **434**, 39 (1995), [Erratum-ibid. B **444**, 447 (1995)], [arXiv:hep-ph/9406421].

[53] A. Ali, H. Asatrian and C. Greub, Phys. Lett. B **429**, 87 (1998), [arXiv:hep-ph/9803314].

[54] H. M. Asatrian, G. K. Yegiian and A. N. Ioannisian, Phys. Lett. B **399**, 303 (1997).

[55] H. H. Asatrian and H. M. Asatrian, Phys. Lett. B **460**, 148 (1999), [arXiv:hep-ph/9906221].

[56] H. H. Asatryan, H. M. Asatrian, G. K. Yeghiyan and G. K. Savvidy, Int. J. Mod. Phys. A **16**, 3805 (2001), [arXiv:hep-ph/0012085].

[57] A. G. Akeroyd, Y. Y. Keum and S. Recksiegel, Phys. Lett. B **507**, 252 (2001), [arXiv:hep-ph/0103008].

[58] A. G. Akeroyd and S. Recksiegel, [arXiv:hep-ph/0109091].

[59] M. Tanaka, Z. Phys. C **67**, 321 (1995), [arXiv:hep-ph/9411405].

[60] T. Miura and M. Tanaka, Talk given at Workshop on Higher Luminosity B Factory, Tsukuba, Japan, 23-24 Aug 2001, [arXiv:hep-ph/0109244].

[61] R. Barbieri, L. J. Hall and A. Strumia, Nucl. Phys. B **445**, 219 (1995), [arXiv:hep-ph/9501334].

[62] J. Hisano, T. Moroi, K. Tobe and M. Yamaguchi, Phys. Rev. D **53**, 2442 (1996), [arXiv:hep-ph/9510309].

[63] J. Hisano and D. Nomura, Phys. Rev. D **59**, 116005 (1999), [arXiv:hep-ph/9810479].

[64] R. Kitano and Y. Okada, Phys. Rev. D **63**, 113003 (2001), [arXiv:hep-ph/0012040].

[65] D. E. Groom *et al.* (Particle Data Group), Eur. Phys. J. C **15**, 1 (2000).

[66] W. Bernreuther, O. Nachtmann and P. Overmann, Phys. Rev. D **48**, 78 (1993).

[67] S. Y. Choi, K. Hagiwara and M. Tanabashi, Phys. Rev. D **52**, 1614 (1995), [arXiv:hep-ph/9412203].

[68] Y. S. Tsai, Phys. Rev. D **51**, 3172 (1995), [arXiv:hep-ph/9410265].

[69] J. H. Kuhn and E. Mirkes, Phys. Lett. B **398**, 407 (1997), [arXiv:hep-ph/9609502].

[70] U. Kilian, J. G. Korner, K. Schilcher and Y. L. Wu, Z. Phys. C **62**, 413 (1994).

[71] A. Falk *et al.*, [arXiv:hep-ph/0110317].

[72] R. Godang *et al.*, Phys. Rev. Lett. **84**, 5038 (2000), [arXiv:hep-ex/0001060].

[73] S. Bergmann *et al.*, Phys. Lett. B **486**, 418 (2000), [arXiv: hep-ph/0005181].

[74] G. Blaylock et al., Phys. Lett. B **355**, 555 (1995), [arXiv:hep-ph/9504306].

[75] M. Gronau, Y. Grossman and J. Rosner, Phys. Lett. B **508**, 37 (2001), [arXiv:hep-ph/0103110].

[76] E. Golowich and S. Pakvasa, Phys. Lett. B **505**, 94 (2001),[arXiv:hep-ph/0102068].

[77] L. Wolfenstein, Phys. Rev. Lett. **75**, 2460 (1995), [arXiv:hep-ph/9505285].

[78] G. Burdman, E. Golowich, J. Hewett and S. Pakvasa, [arXiv:hep-ph0112235].

[79] KEKB Design Report, KEK Report 95-7.

[80] F.Zimmermann, SL-Note-2000-004 AP (2000).

[81] Y. Suetsugu et al., Proc. of PAC2001, Chicago, June 18-22, 2001.

[82] K. Ohmi and F. Zimmermann, Phy. Rev. Let. **85** (2000) 3821-3824.

[83] M. Q. Barton, Nuc. Ins. Meth. **A243** (1986) 278.

[84] KEK B-Factory Design Report, KEK Report 95-7 (1995): H. Fukuma *et al.*, European Particle Accelerator Conference (2000), K. Akai, *et al.*, "COMMISSIONING OF THE KEKB B-FACTORY", WEAR4, Proc. 1999 Particle Accelerator Conference, New York(1999); K. Akai, *et al.*, "COMMISSIONING OF THE KEKB B-FACTORY", Proc. Intl. Workshop on e+e- Factories E. Kikutani.(1999); H. Fukuma, et al., "OBSERVATION OF VERTICAL BEAM BLOW-UP IN KEKB LOW ENERGY RING", Proc. 2000 European Particle Accelerator Conference, Vienna(2000); Y. Funakoshi, *et al.*, "KEKB PERFORMANCE", Proc. 2000 European Particle Accelerator Conference, Vienna(2000).

[85] Belle Collaboration, KEK Report 2000-4 (2000), to be published in Nucl. Instrum. Method.

[86] H. Hirano *et al.*, Nucl. Instrum. Methods **A455**, 294 (2000); M. Akatsu *et al.*, Nucl. Instrum. Methods **A454**, 322 (2000).

[87] G. Alimonti *et al.*, Nucl. Instr. and .Meth. **A453**, 71 (2000).

[88] H. Kichimi *et al.*, Nucl. Instr. and Meth. **A453**, 315 (2000).

[89] T. Iijima *et al.*, Nucl. Instr. and Meth. **A453**, 321 (2000).

[90] H. Ikeda *et al.*, Nucl. Instr. and Meth. **A441**, 401 (2000).

[91] K. Hanagaki *et al.*, submitted to Nucl. Instr. and Meth., [arXiv:hep-ex/0108044].

[92] A.Abashian *et al.*, Nucl. Instr. and .Meth. **A449**, 112 (2000).

[93] S.K.Sahu et al., Nucl. Instr. and Meth. **A382** (1996) 441.

[94] Hamamatsu Photonics K.K., "Photomultiplier Tubes – basics and applications –", 2nd edition, 1999.

[95] M.Akatsu et al., Nucl. Instr. and Meth. **A440** (2000) 123.; T.Ohshima, Nucl. Instr. and Meth. **A453** (2000) 331.; M.Hirose et al., Nucl. Instr. and Meth. **A460** (2001) 326.

[96] I.Adachi et al., Nucl. Instr. and Meth. **A355** (1995) 390.; T.Iijima et al., Nucl. Instr. and Meth. **A453** (2000) 321.; T.Sumiyoshi et al., Nucl. Instr. and Meth. **A433** (1999) 385., and references therein.

[97] E.Aschenauer et al., Nucl. Instr. and Meth. **A440** (2000) 338.

[98] LHCb Collaboration, "LHCb RICH: Technical Design Report", CERN-LHCC-2000-037.

[99] KEK Progress Report 97-1.

[100] M. Nakao, M. Yamauchi, S. Y. Suzuki, R. Itoh and H. Fujii, *IEEE Trans. on Nucl. Sci.*, vol. 47, no. 2, pp. 56–60, Apr. 2000.

[101] M. Nakao *et al.*, talk given at the IEEE NSS, Lyon, Oct 2000, to be appeared in *IEEE Trans. on Nucl. Sci.*